Technical Report No. 201

03674-24-T

TRIBAND: THE THREE BAND FILTER FOR THE CONTINUING MIMI EXPERIMENT

by

Norman Hatter

Approved by: *Theodore G. Birdsall*

Theodore G. Birdsall

for

COOLEY ELECTRONICS LABORATORY

Department of Electrical Engineering
The University of Michigan
Ann Arbor, Michigan

ABSTRACT

An experiment was conducted as part of the continuing study of sound propagation in the Straits of Florida. A 420-Hz continuous wave (CW) signal was transmitted, received at the 7-mile hydrophone, and processed by the Linc-8 on-line digital processor. The processing yielded the magnitude and phase of the reception in a 1/16-Hz band, the magnitude of the reception in a 1-Hz band but excluding the 1/16-Hz band, and the magnitude of the reception in a 16-Hz band that excluded the 1-Hz band. All bands were centered at 420 Hz.

The purposes of the experiment were to verify the possibility of such a three-band analysis and to obtain "typical" relative power ratios to aid in the design of analog triband phase coherent demodulation.

ACKNOWLEDGEMENTS

TABLE OF CONTENTS

LIST OF ILLUSTRATIONS

LIST OF ILLUSTRATIONS (Cont.)

1. INTRODUCTION

1.1 MIMI Description

The project MIMI is a joint experimental effort of the Acoustics Group of The Institute of Marine Sciences (IMS), University of Miami, (MIMI-A), and the Stochastic Signal Processing Group, Cooley Electronics Laboratory (CEL), University of Michigan, (MIMI-C). The nickname "MIMI" was generated by concatenating the first two letters of both Miami and Michigan.

The acoustic and environmental test facility is maintained and operated by MIMI-A, which is also responsible for the majority of the environmental studies and propagation studies. MIMI-C is responsible for the development of signal processing techniques to improve the reliability and relevance of the experimental propagation data.

The signal source is a flextensional transducer mounted at the focus of a 24 ft compliant-tube parabolic reflector. The whole assembly is located off Fowey Rocks at a depth of 85 ft (Ref. 1).

The experimental channel used in this study is that portion of the Straits of Florida approximately located between Fowey Rocks and the "seven-mile" hydrophone. The relevant features of the channel are illustrated in Fig. 1. The bottom profile shows a 350 meter deep shelf just beyond the hydrophone. In addition to added interference
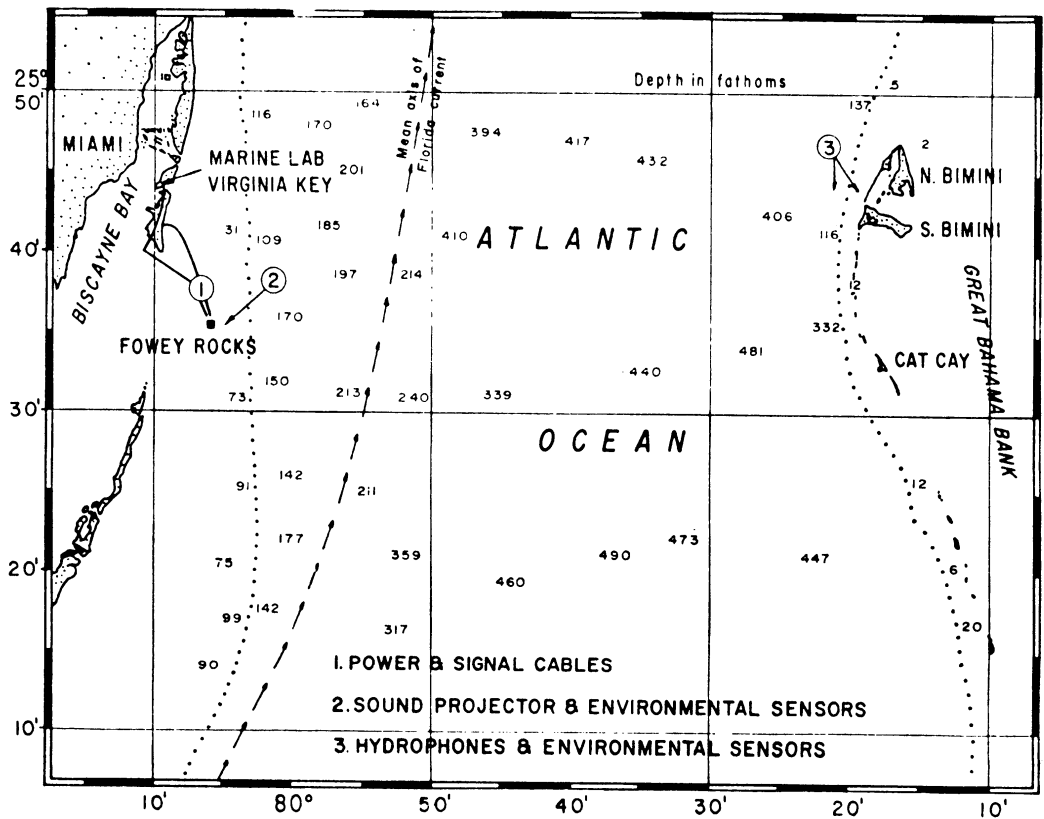
Fig. 1 (a) Straits of Florida, Miami to Bimini
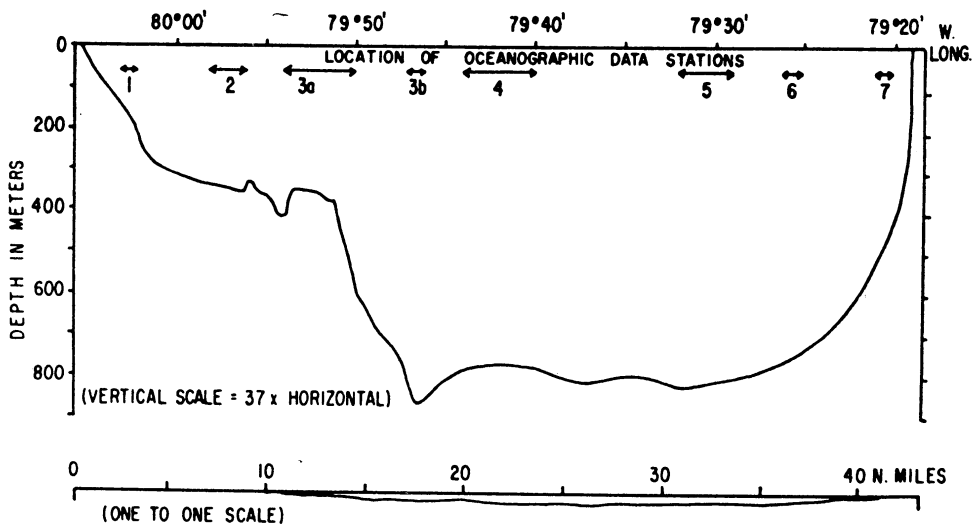
Fig. 1 (b) Bottom Profile, Fowey Rocks to Bimini

from biological noise, surface related noise, and shipping noise, the signal is distorted by the slowly changing multipath structure and the rapidly changing instantaneous position of the surface. A quantitative measurement of the effects of this last, the surface waves, is one of the purposes of the triband processing.

The data acquisition devices consist of the hydrophone, seven miles of underwater cable and its amplifiers, a telephone line from Fowey Rocks to MIMI-A and the terminal amplifiers there, and then in parallel, amplifiers and filters to a phase coherent demodulator, Sanborn strip chart recorders, and two on-line Linc-8 digital computers. One digital computer was used as the primary processing device for this experiment. Figure 2 shows the overall system configuration.

1.2 Proposed Model

From the earliest MIMI studies, and continually on all studies at all phones, the effect of the surface waves as a source of modulation has been evident. Power spectra of continuous wave (CW) amplitude fluctuations, carrier phase fluctuations, and local wave height all coincide in shape, although differing in magnitude. This is a well-known phenomena, well understood in-the-small (one surface interaction, small ensonified area) but not often quantitatively measured or modeled to the extent necessary for prediction.

3

Examination of Sanborn strip chart records of the received CW amplitude and phase indicate that the major effect is an amplitude modulation (AM), with some minor phase modulation (PM). Both AM and small angle PM primarily produce first order sidebands. The wave periods at MIMI have 2 second to 10 second periods, giving rise to sidebands of 0.1 Hz to 0.5 Hz on either side of every transmitted spectral line. Most MIMI processing has used narrower filters for CW or narrow tooth comb filters for sequence transmissions to eliminate this modulation effect from the analysis.

Therefore we have been confident that this surface-wave-modulation is present, but have no quantitative measurement to establish its magnitude or to study its behavior under changing conditions. The primary purpose of triband analysis is to obtain such quantitative measurements.

Continuing studies of the MIMI 7-mile and 42-mile channels almost invariably measure two types of carrier power fluctuation sharp, deep fades typical of multipath destructive phase interference with recurrences of the order of 15 to 60 minutes, and gross level changes in the maximum "between-fade" levels with changes spread either over months or occasionally with rapid transition in a few hours. The second purpose of triband analysis is aimed at the type of fade with the 15 to 60 minute recurrence. Are these fades accompanied by an increase in the power in the surface-wave sideband region ±0.5 Hz off

4

carrier? If this occurs, the implication would be that the carrier was being angle modulated by the waves present. It is well known that for the case of pure angle modulation, the total power remains constant; it is merely exchanged between the carrier and its modulation sidebands.
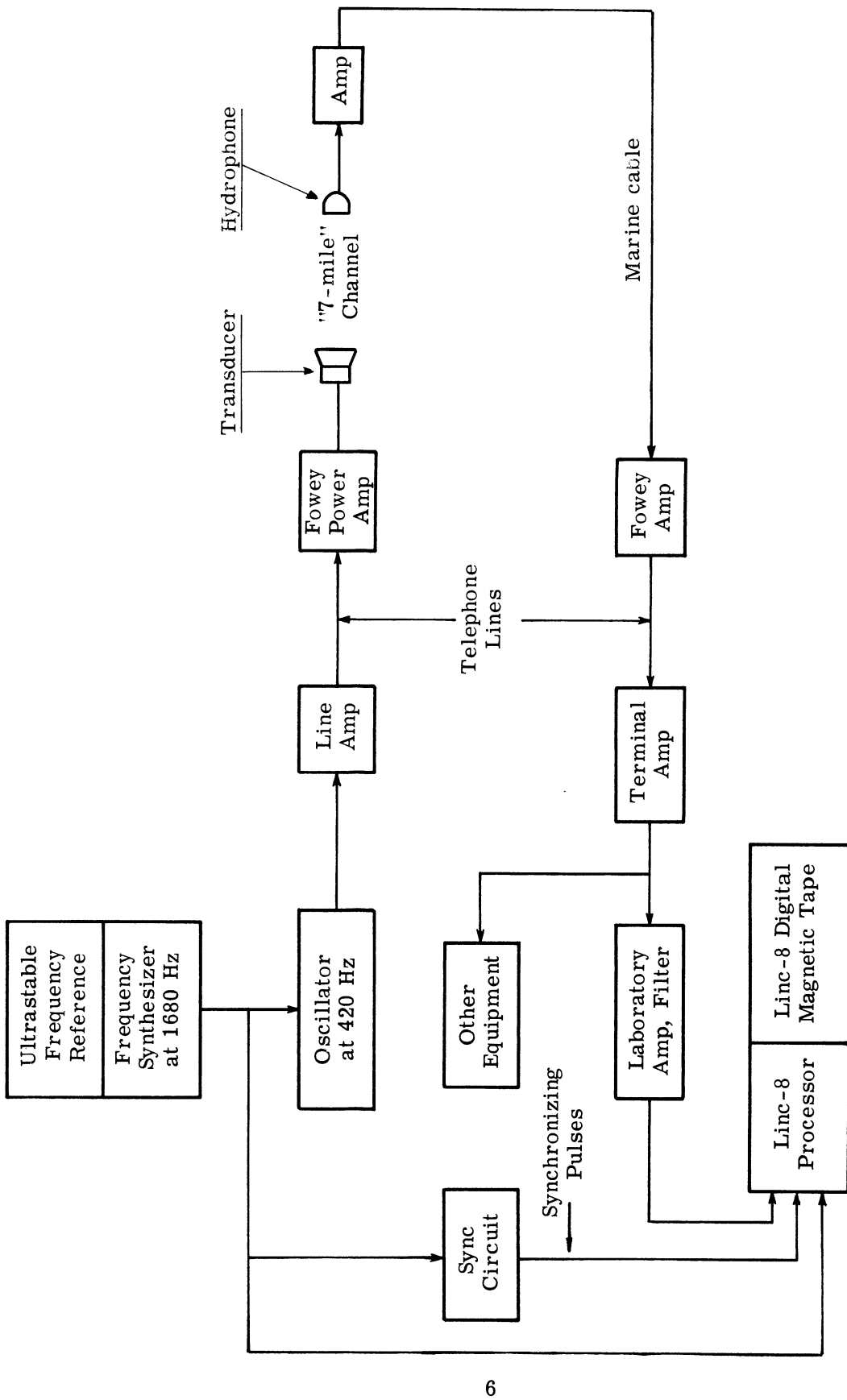
Fig. 2. Triband experimental system

2. BACKGROUND AND PURPOSE

In this experiment, the signal from the channel is separated into carrier and sideband components. The sidebands are further divided into a narrow sideband (nsb) and a wide sideband (wsb). The power in each band is calculated and averaged over a fixed time period. The correlation coefficient for these samples was calculated and examined. If the proposed model is correct, a strong negative correlation between the carrier power and the sideband power is expected. The use of a three-band filter gives rise to the nickname "TRIBAND".

2.1 The Experiment

The experiment called for a 420-Hz continuous wave signal to be transmitted through the channel. The signal would then be received and digitally processed.

The MIMI project is unique in that measurements are made between two fixed sites, thus eliminating the necessity of correcting for drifting sites. The transmitter consists of precision oscillator (1 part in 10^{10}) from which the 1680-Hz clock frequency is derived. The 1680 Hz is further divided to 420 Hz which is then transmitted by cable to the amplifiers at Fowey Rocks lighthouse. The amplifier output is then coupled, by cable, to the transducer. The piezo-electric hydrophone receives the signal which is then conducted to IMS via cable. At IMS the receiver signal is amplified to a range of

less than ±1V in order that the input to the fixed bandpass filter and the A/D converter is not exceeded. From there, the signal is passed through a passive, fixed filter with a 120-Hz passband centered at 420 Hz and sampled by the A/D converter for subsequent digital processing. After processing,the digital data is written onto magnetic tape for post-processing. The data is also typed out on a teletype for correlation with the taped data.

Our primary concern will be with the signal after it has been received at IMS. A synchronizing signal is provided to ensure that phase coherency is maintained. The 1680 Hz is also used to sample the signal waveform. Ideally, the 420-Hz signal is sampled four times per cycle which is more than adequate to recover all of the information and is exactly four times the carrier frequency to facilitate demodulation. The computer then performs the filtering in accordance with the description in Section 2.5.

2.2 Bandpass Filter Implementation

The concept of the filters for the experiment is sketched in Fig. 3.

$$H_{LP}(f) \approx \begin{cases} 1 & |f| < f_1 \\ 0 & \text{elsewhere} \end{cases}$$

$$H_{BP_1}(f) \approx \begin{cases} 1 & f_1 \leq |f| < f_2 \\ 0 & \text{elsewhere} \end{cases}$$

$$H_{BP_2}(f) \approx \begin{cases} 1 & f_2 \leq |f| < f_3 \\ 0 & \text{elsewhere} \end{cases}$$
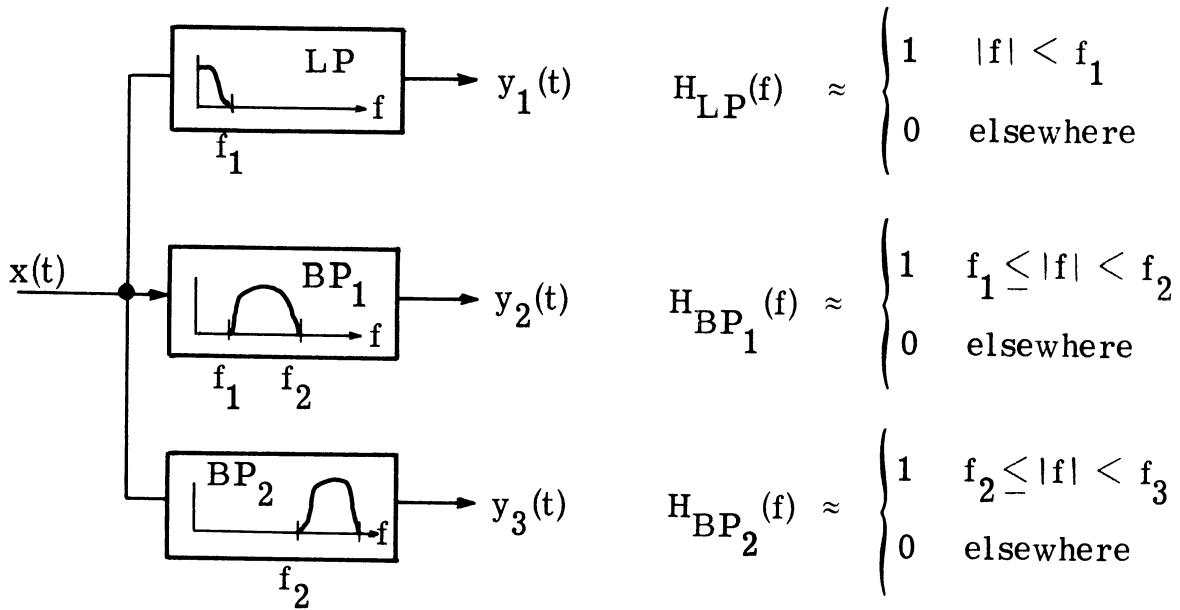
Fig. 3. Three band filter

The implementation of the bandpass filters posed the most difficult problem. The bandpass filters might be realized by using the following scheme:

9
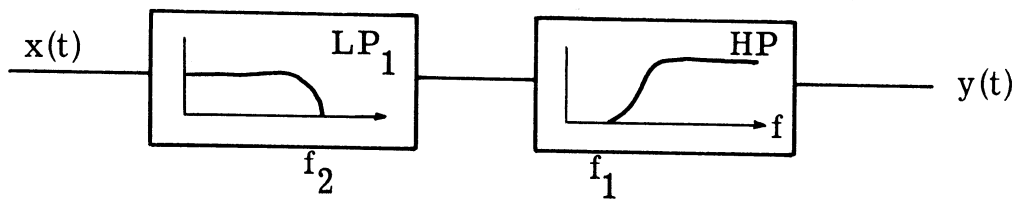
Fig. 4. One bandpass filter implementation

That is, a low pass filter and a high pass filter are cascaded

to form the bandpass filter (Fig. 4). The same effect could be achieved by

combining two low pass filters as in Fig. 5 .
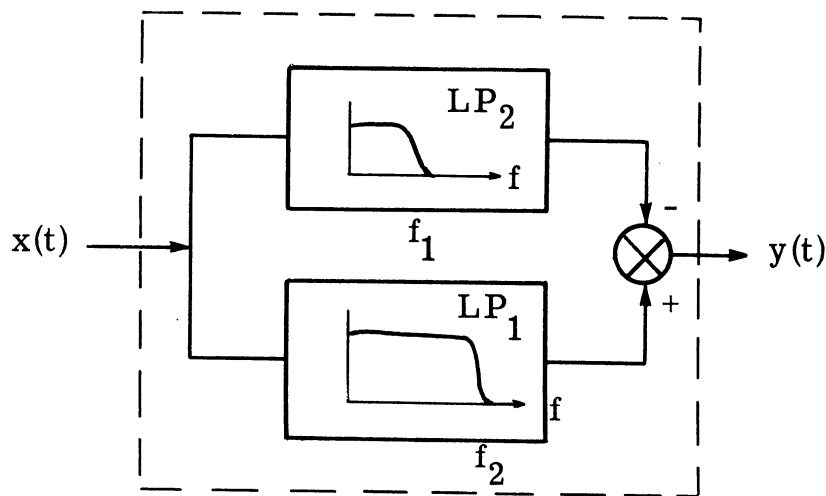
Fig. 5. Another bandpass filter implementation

The output of the narrower filter is subtracted from the output

of the wider filter forming a bandpass filter. For ease of digital im-

plementation, this is the method that was chosen.

10

2.3 Analog Filters

Consider the analog filter which is analogous to the digital process (Fig. 6). The proposed filter would have impulse response:

$$h(t, \tau) = 1/\tau \qquad |t| < \tau/2$$
$$0 \qquad |t| > \tau/2 \qquad (1)$$
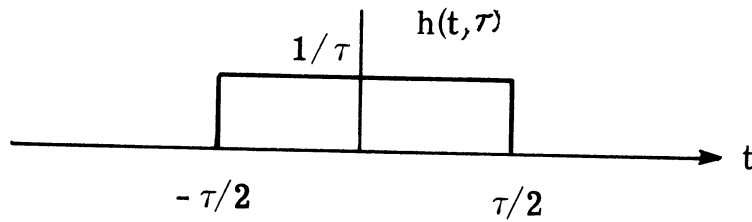
Fig. 6. Analog filter impulse response

This filter may be realized if sufficient delay is incorporated. The transfer function is

$$H(f, \tau) = \int_{-\infty}^{\infty} h(t, \tau) e^{-j\omega t} \, dt$$

$$= \frac{1}{\tau} \int_{-\frac{\tau}{2}}^{\frac{\tau}{2}} e^{-j\omega t} \, dt$$

where

$$j = \sqrt{-1}$$

$$\omega = 2\pi f$$

$$H(f, \tau) = \frac{2}{\tau} \int_0^{\tau/2} \cos \omega t \, dt$$

$$= \frac{2}{\omega \tau} \left[\sin \omega t \right]_0^{\tau/2}$$

$$= \frac{2}{2\pi f \tau} \left[\sin \frac{2\pi f \tau}{2} \right]$$

$$= \frac{\sin \pi f \tau}{\pi f \tau} = \text{sinc} (f \tau) \tag{2}$$

If two low pass filters are combined as illustrated in Fig. 5, one having m times the averaging time of the other, the transfer function for the combination becomes

$$H_c(f, \tau) = \int_{-\infty}^{\infty} h_c(t, \tau) \, e^{-j\omega t} \, dt$$

$$= \text{sinc} (f\tau) - \text{sinc} (fm\tau) \tag{3}$$

where

$$h_c(t, \tau) = h_1(t, \tau) - h_2(t, \tau)$$

This function can be factored to yield the corresponding high pass and low pass filters as in Fig. 4.

$$H_c(f, \tau) = \text{sinc} (f\tau) - \text{sinc} (fm\tau)$$

$$H_c(f, \tau) = \frac{\sin \pi f \tau}{\pi f \tau} - \frac{\sin \pi f m \tau}{\pi f m \tau}$$

$$\tag{4}$$

$$= \frac{\sin \pi f \tau}{\pi f \tau} \left[1 - \frac{\sin \pi m f \tau}{m \sin \pi f \tau} \right] = H_{LP}(f, \tau) \, H_{HP}(f, m\tau)$$

The power transfer function of the high pass filter is:

$$H^2_{HP}(f, m\tau) = \left[1 - \frac{\sin \pi m f \tau}{m \sin \pi f \tau} \right]^2 \qquad (5)$$

The important characteristics of the high pass filter are:

First, $\qquad H_{HP}(f) = 0 \implies \dfrac{\sin \pi m f \tau}{m \sin \pi f \tau} = 1 \qquad (6)$

or

$$\sin \pi m f \tau = m \sin \pi f \tau \qquad (7)$$

which only occurs when $f\tau$ is an integer. In particular, at $f = 0$, the power transfer is zero.

$$H^2_{HP}(0) = 0 \qquad (8)$$

Second, $H_{HP}(f, m\tau) = 1 \implies \sin \pi m f \tau / m \sin \pi f \tau = 0$

or

$$\sin \pi m f \tau = 0 \implies \pi m f \tau = k \pi$$

$$\implies f = k/m\tau$$

Hence,

$$H^2_{HP}(k/m\tau) = 1, \quad k = 1, 2, \ldots, m-1 \qquad (9)$$

For $\tau = 1/16$ and $m = 16$, the 3 dB bandwidth of the reject region about dc is approximately 1.4 Hz.

13

$$\left[1 - \frac{\sin \pi f}{16 \sin \left(\frac{\pi f}{16} \right)} \right]^2$$

$$1 - \left[\frac{\sin \pi f}{16 \sin \left(\frac{\pi f}{16} \right)} \right]^2$$
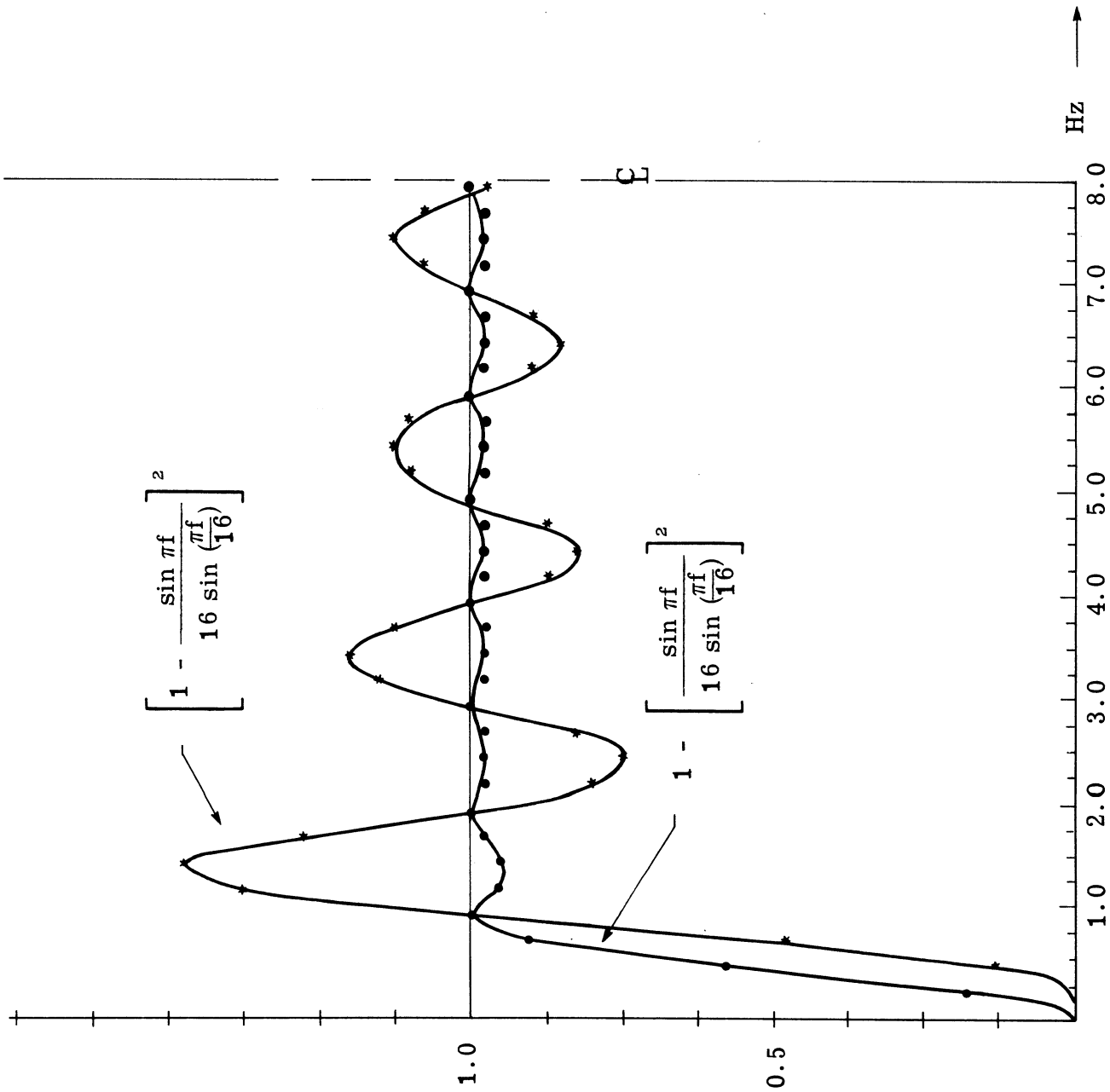
Fig. 7. High-pass filter power transfer chart

14

The "overshoot" of the high pass filter for m = 16 is approximately 47 percent and occurs at a frequency of about 1.5 Hz (Fig. 7).

2.4 Digital Block Averaging

The objective is to obtain a bandpass filter by differencing two low pass filters. For our processing, the averaging time of the digital narrow band low pass filter was 16 times the averaging time of the digital wide band low pass filter. This means that for each value out of the narrow filter, there were 16 values out of the wide filter. That is, there was one value from each of 16 wide filters which were selected sequentially in time during the averaging period of the narrow filter. Although this digital situation is similar to the analog just considered, the processing is not time invariant. The output of the narrow filter will have to be subtracted from each of the outputs of the 16 wide filters. This method of processing is called a "block averaging" or a "synchronous, cyclostationary" technique. The analog impulse responses are illustrated in Fig. 8.

These impulse responses are not realizable, but may be made so by allowing sufficient delay. The required delays are given in Eq. 10, where:

(a) $1/2 \tau$ is the delay necessary to make each wide filter realizable,

(b) $k \tau$ is the delay necessary to pick the appropriate output for differencing, and
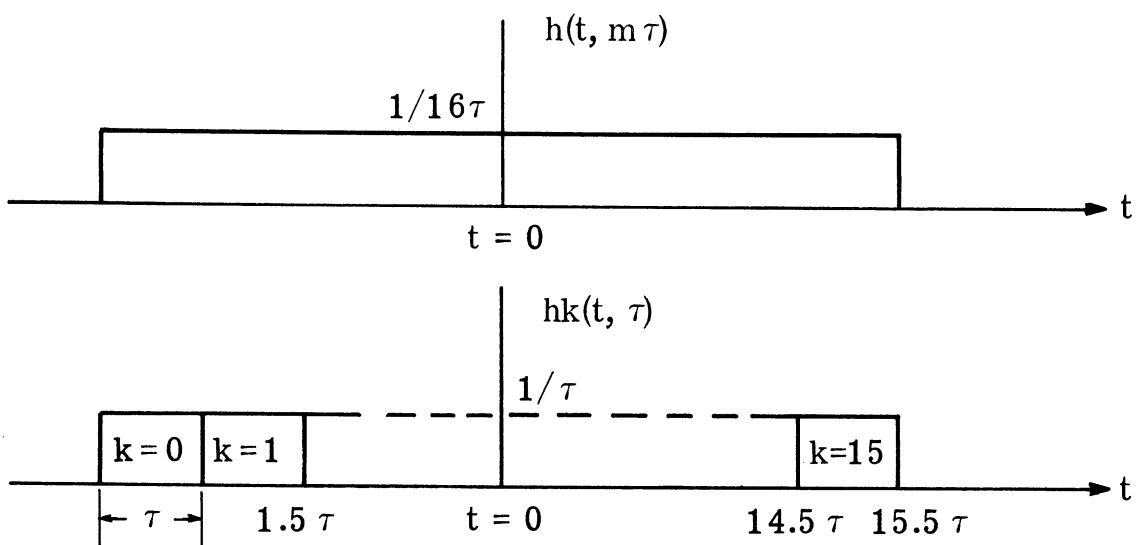
Fig. 8. Analog filter impulse responses

(c) 8τ is the delay necessary to make the narrow filter realizable.

$$h_k(\tau) = h[t - (k+\tfrac{1}{2})\tau; \tau] - h(t - 8\tau; 16\tau); \quad k = 0, 1, \ldots, 15$$

(10)

The transfer function for Eq. 10 is:

$$H_k(f) = \exp[-j2\pi(k+\tfrac{1}{2})f\tau]\,\mathrm{sinc}(f\tau) - \exp(-j16\pi f\tau)\,\mathrm{sinc}(16f\tau)$$

(11)

$$H_k(f) = \exp(-j16\pi f\tau)\,\mathrm{sinc}(f\tau)\left[\exp[j\pi(15 - 2k)f\tau] - \frac{\sin(16\pi f\tau)}{16\sin(\pi f\tau)}\right]$$

where $H_k(f)$ has been factored into a low pass and high pass product. The power transfer characteristic of the low pass filter is the familiar $\mathrm{sinc}^2(f\tau)$ function. The high-pass filter power transfer characteristic is a function of the delay, k.

16

$$\left| H_{HP,k}(f) \right|^2 = \left| \exp[j\pi(15 - 2k)f\tau] - \frac{\sin(\pi 16 f\tau)}{16\sin(\pi f\tau)} \right|^2 \tag{12}$$

Recall: $\qquad |H|^2 = H\,H^* \qquad$ (H complex) $\tag{13}$

and

$$\left| e^{j\alpha} - \beta \right|^2 = (e^{j\alpha} - \beta)(e^{-j\alpha} - \beta)$$

$$= 1 + \beta^2 - \beta(e^{j\alpha} + e^{-j\alpha})$$

$$= 1 + \beta^2 - 2\beta\cos\alpha \tag{14}$$

Therefore, a more convenient form of the high pass power transfer characteristic is the real equation

$$\left| H_{HP,k}(f) \right|^2 = 1 + \left[\frac{\sin(\pi 16 f\tau)}{16\sin(\pi f\tau)} \right]^2 - 2\,\frac{\sin(\pi 16 f\tau)}{16\sin(\pi f\tau)}\cos(15-2k)\pi f\tau$$

$$k = 0, 1, \ldots, 15 \tag{15}$$

The individual power transfer characteristics for k = 0, 1,

..., 15 have been plotted and are given in Appendix B. It is evident

that each of them varies about the desired rectangular pass band.

However, our processing calls for a fairly rectangular pass band with

variations reduced to a minimum.

In our processing, we are interested in the power in the band.

We estimate the power by averaging the magnitude squared of the output

17

of 16 outputs. Hence, we look at the average of the individual power transfer characteristics which is averaged over the 16 delays in the block averaging process.* Accordingly, the bandpass power transfer function is the average of the individual bandpass power transfer functions that are a function of the delay, k. Using this approach, we see from Eq. 11, that only the high pass filter is a function of the delay, k. The low-pass filter is merely the $\text{sinc}^2(f\tau)$, unconditional upon k. From Eq. 15, it is noted that the third term is the only one which is affected by k. Accordingly, we shall average over the cosine term.

The average value of a set of cosines at uniformly spaced frequencies and symmetric about zero is

$$\frac{1}{16} \sum_{k=0}^{15} \cos \pi(15-2k)\, f\tau = \frac{\sin \pi\, 16\, f\tau}{16 \sin \pi f\tau} \tag{16}$$

From which,

$$\left|H_{HP}(f)\right|^2 = \frac{1}{16} \sum_{k=0}^{15} \left|H_{BP,K}(f)\right|^2 = 1 - \left(\frac{\sin \pi m f\tau}{m \sin \pi f\tau}\right)^2 \tag{17}$$

This average high-pass power transfer characteristic is plotted in Fig. 7 and also in Fig. 9.

---

*See Appendix A for development.
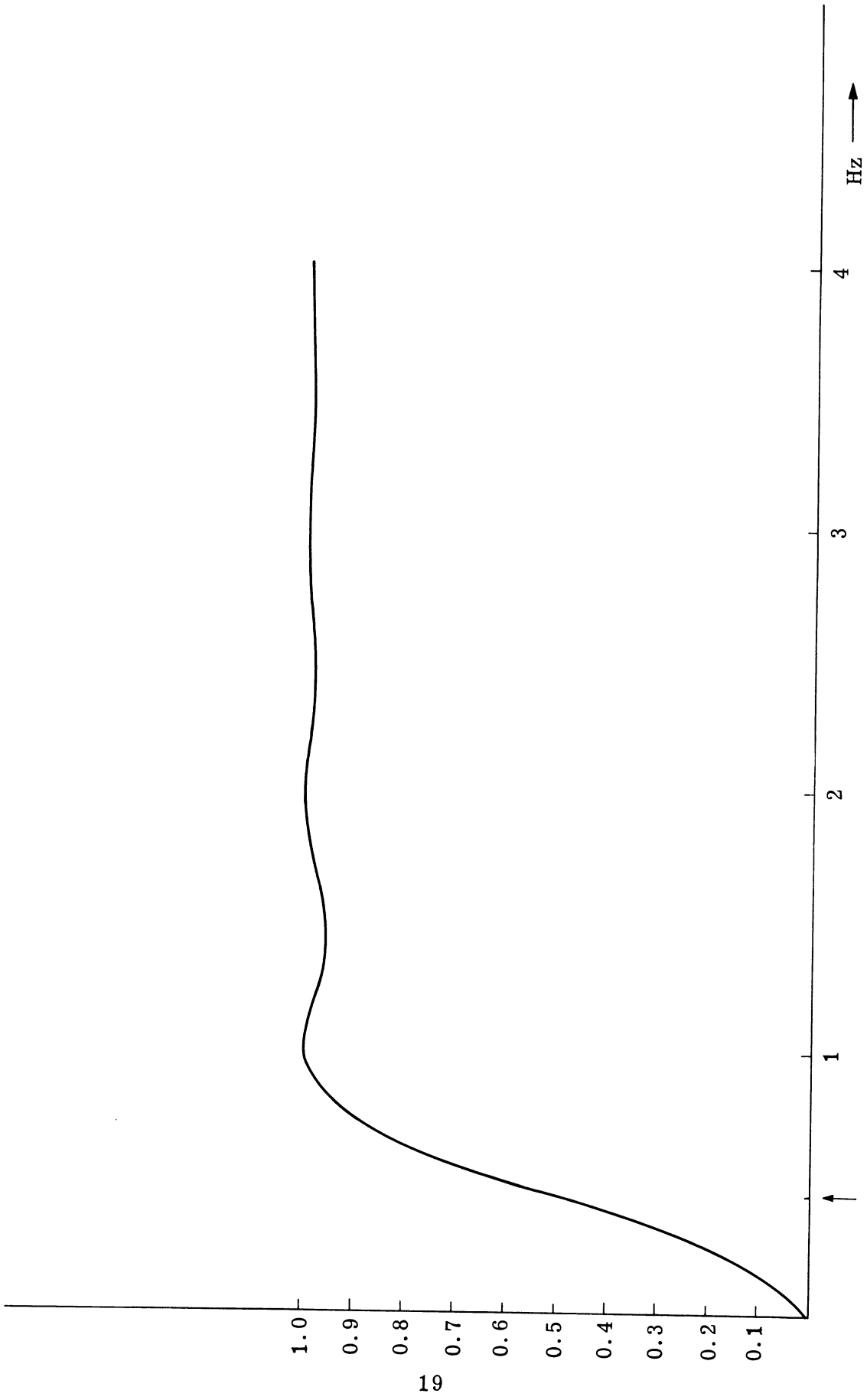
Fig. 9.   Average high-pass power   **M** = 16
           Transfer characteristic

19

To obtain the bandpass power transfer characteristic we use Eq. 17 and Eq. 12.

$$\left| H_{BP}^{(f)} \right|^2 = \left| H_{LP}^{(f)} \right|^2 \left| H_{HP}^{(f)} \right|^2 \tag{18}$$

$$\left| H_{BP}^{(f)} \right|^2 = \left(\frac{\sin \pi f \tau}{\pi f \tau} \right)^2 \left[1 - \left(\frac{\sin \pi m f \tau}{m \sin \pi f \tau} \right)^2 \right] \tag{19}$$

$$\left| H_{BP}^{(f)} \right|^2 = \text{sinc}^2 (f \tau) - \text{sinc}^2 (m f \tau) \tag{20}$$

Equation 20 is the bandpass power transfer characteristic of interest and turns out to be simply the difference of two sinc^2 functions which is the power transfer function of the bandpass filters described in Section 2. Figure 10 is a plot of the bandpass power transfer characteristic.

```
**********
1.47527E-04
1.51551E-03
1.21834E-02
1.43762E-02
1.68059E-02
1.99138E-02
1.14248E-01
1.19380E-01
1.24812E-01
1.31070E-01
1.38756E-01
1.47373E-01
1.56309E-01
1.66151E-01
1.77515E-01
1.90635E-01
1.10738E+00
1.11643E+00
1.13182E+00
1.14820E+00
1.16459E+00
1.18076E+00
1.20127E+00
1.22140E+00
1.24135E+00
1.26064E+00
1.28455E+00
1.30804E+00
1.33083E+00
1.35416E+00
1.37543E+00
1.40528E+00
1.42967E+00
1.45489E+00
1.48189E+00
1.50920E+00
1.53457E+00
1.55975E+00
1.58735E+00
1.61499E+00
1.63558E+00
1.65557E+00
1.69051E+00
1.71725E+00
1.73942E+00
1.76035E+00
1.78555E+00
1.81057E+00
1.83325E+00
1.84589E+00
1.86652E+00
1.83955E+00
1.89928E+00
1.90601E+00
1.92660E+00
1.94964E+00
1.94472E+00
1.92635E+00
1.94766E+00
1.98713E+00
1.90732E+00
1.91515E+00
1.88653E+00
```

$$\left[\frac{\sin\left(\frac{\pi f}{16}\right)}{\frac{\pi f}{16}}\right]^2 \left[1 - \left(\frac{\sin \pi f}{16 \sin\left(\frac{\pi f}{16}\right)}\right)^2\right]$$

$Hz \longrightarrow$

1.0 2.0 3.0 4.0 5.0 6.0

1.0 0.5 0.0

Fig. 10. Bandpass power transfer characteristic

2.5 The Digital Process

The signal is digitally demodulated and then summed to obtain

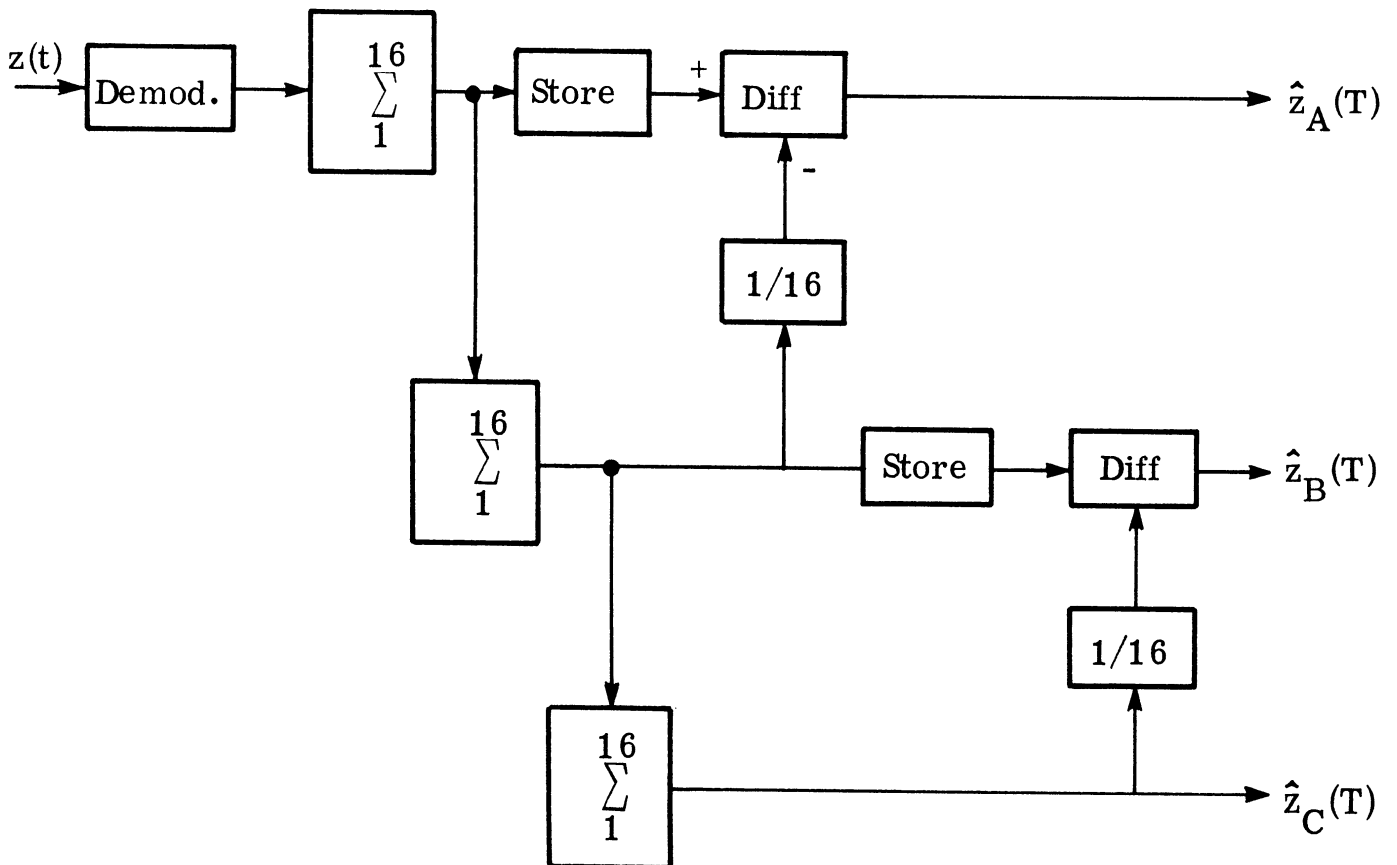the desired outputs. Figure 11 is a block diagram of the process.

Fig. 11. Partial digital process

The signal is sampled at the 1680 Hz clock frequency. Prior

to sampling, the analog signal is passed through an analog filter with

a 160 Hz bandpass centered at 420 Hz. Hence, an alias is avoided since signal components of 840 Hz and above are negligible. The demodulation process essentially shifts the band of interest down to dc. The transfer function (Ref. 2) of the demodulation process is

$$H(f) = j e^{-j2\pi \hat{T}} \frac{\sin 4\pi f \hat{T}}{\cos \pi f \hat{T}} \tag{25a}$$

$$|H(f)| = \frac{|\sin 4\pi f \hat{T}|}{|\cos \pi f \hat{T}|} \tag{25b}$$

$$\hat{T} = 1/1680 \text{ sec}$$

The output rate from the demodulation process is 210 complex values/sec.

The summation may be viewed as a filter whose impulse response is a string of impulse functions (Fig. 12).
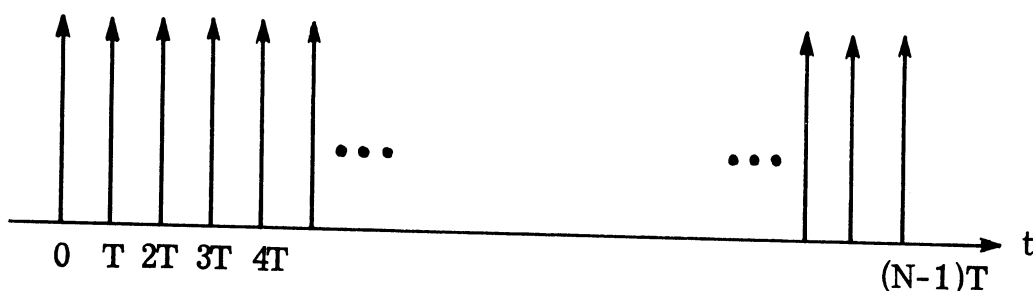
$$T = 1/210 \text{ sec}$$

Fig. 12. Summation impulses

23

As a digital filter, the response is:

$$h(t) = \sum_{n=0}^{N-1} \delta(t - nT) \tag{26}$$

The transfer function is:

$$H(f) = \int_{n=0}^{(N-1)T} \sum \delta(t - nT) \, e^{-j2\pi ft} \, dt$$

$$= \sum_{n=0}^{(N-1)} \int_0^{(N-1)T} \delta(t - nT) \, e^{-j2\pi ft} \, dt$$

$$= \sum_{n=0}^{N-1} e^{-j2\pi fnT} \tag{27}$$

Recall:

$$1 + x + x^2 + \ldots + x^n \equiv \frac{1 - x^{n+1}}{1 - x} \; ; \quad x < 1 \tag{28}$$

Therefore,

$$H(f) = \frac{1 - e^{-j2\pi fNT}}{1 - e^{-j2\pi fT}}$$

$$= \frac{e^{-j\pi fNT} \left(e^{j\pi fNT} - e^{-j\pi fNT} \right)}{e^{-j\pi fT} \left(e^{j\pi fT} - e^{-j\pi fT} \right)}$$

$$= e^{-j\pi f(N-1)T} \frac{\sin(\pi fNT)}{\sin(\pi fT)} \tag{29}$$

$$|H(f)| = \frac{|\sin(\pi fNT)|}{|\sin(\pi fT)|} \tag{30}$$

where:

$N = 16$ for the 1st filter $\Longrightarrow NT \simeq 0.08$ sec

$N = 256$ for the 2nd filter $\Longrightarrow NT \simeq 1.22$ sec

$N = 4096$ for the 3rd filter $\Longrightarrow NT \simeq 19.5$ sec

These numbers have step ratios of 16 and were chosen so that the surface wave periods of approximately 2 to 10 seconds fall between $NT = 1.22$ sec and $NT = 19.5$ sec. From Eq. 30 and Fig. 11 it can be seen that the resulting averaged difference power transfer characteristics are

$$|H_3(f)|^2 = \left[\frac{\sin 4096 \, \pi fT}{4096 \sin \pi fT}\right]^2 \tag{31}$$

$$|H_2(f)|^2 = \left[\frac{\sin 256 \, \pi fT}{256 \sin \pi fT}\right]^2 - \left[\frac{\sin 4096 \, \pi fT}{4096 \sin \pi fT}\right]^2 \tag{32}$$

$$|H_1(f)|^2 = \left[\frac{\sin 16 \, \pi fT}{16 \sin \pi fT}\right]^2 - \left[\frac{\sin 256 \, \pi fT}{256 \sin \pi fT}\right]^2 \tag{33}$$
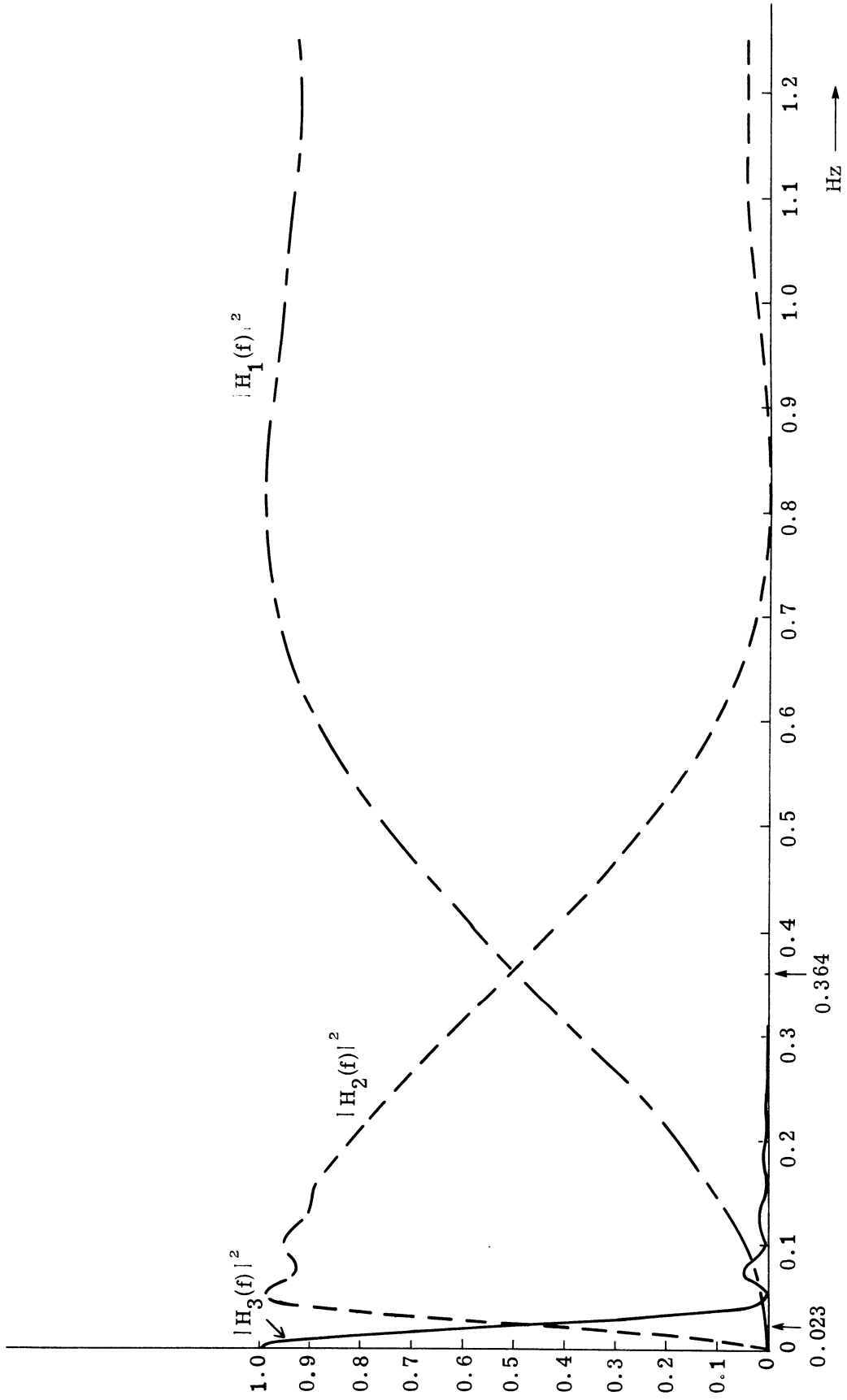
These are plotted in Fig. 13.

25

Fig. 13. Three band filter power transfer characteristic

$H_3(f)$ has a pass band of approximately 50 MHz and is thought to contain primarily carrier energy. $H_2(f)$ is thought to contain both surface modulated energy and some local noise. $H_1(f)$ is thought to contain primarily local noise energy. Notice that the transfer characteristics are periodic in 210 Hz. However, this does not become an important factor since the analog input filter has removed all signals 210 Hz away from the carrier

Figure 14 illustrates the complete digital process. It is understood that the so-called "y" components out of the demodulator go through a process which is identical to that shown for the "x" components. Samples are taken for 19-53/105 seconds which yields 4096 complex values from the demodulator. These values are processed as follows:

$$0 \leq m < 16, \qquad 0 \leq \ell < 256, \qquad 0 \leq k < 4096$$

$$x_1(\ell) = \sum_{k=16\ell}^{16\ell+15} z_0(k) \tag{34}$$

$$x_2(m) = \sum_{\ell=16m}^{16m+15} z_1(\ell) \tag{35}$$

$$x_3 = \sum_{m=0}^{15} z_2(m) \tag{36}$$

$$\hat{x}_1(\ell) = x_1(\ell) - 2^{-4} x_2 \frac{"\ell"}{16} \tag{37}$$

where $\frac{"\ell"}{16}$ = integer part of $\ell/16$

$$\hat{x}_2(m) = x_2(m) - 2^{-4} x_3 \tag{38}$$

$$\tilde{x}_1 = \sum_{\ell=0}^{255} \left(\hat{x}_1(\ell)\right)^2 \tag{39}$$

$$\tilde{x}_2 = \sum_{m=0}^{15} \left(\hat{x}_2(m)\right)^2 \tag{40}$$

$$\hat{P}_1 = \tilde{x}_1 + \tilde{y}_1 \tag{41}$$

$$\hat{P}_2 = \tilde{x}_2 + \tilde{y}_2 \tag{42}$$

$$\hat{P}_3 = (x_3)^2 + (y_3)^2 \tag{43}$$

At this point in the processing, the power estimates $\hat{P}_i$, $i = 1, 2, 3$ are written onto magnetic tape for further processing.
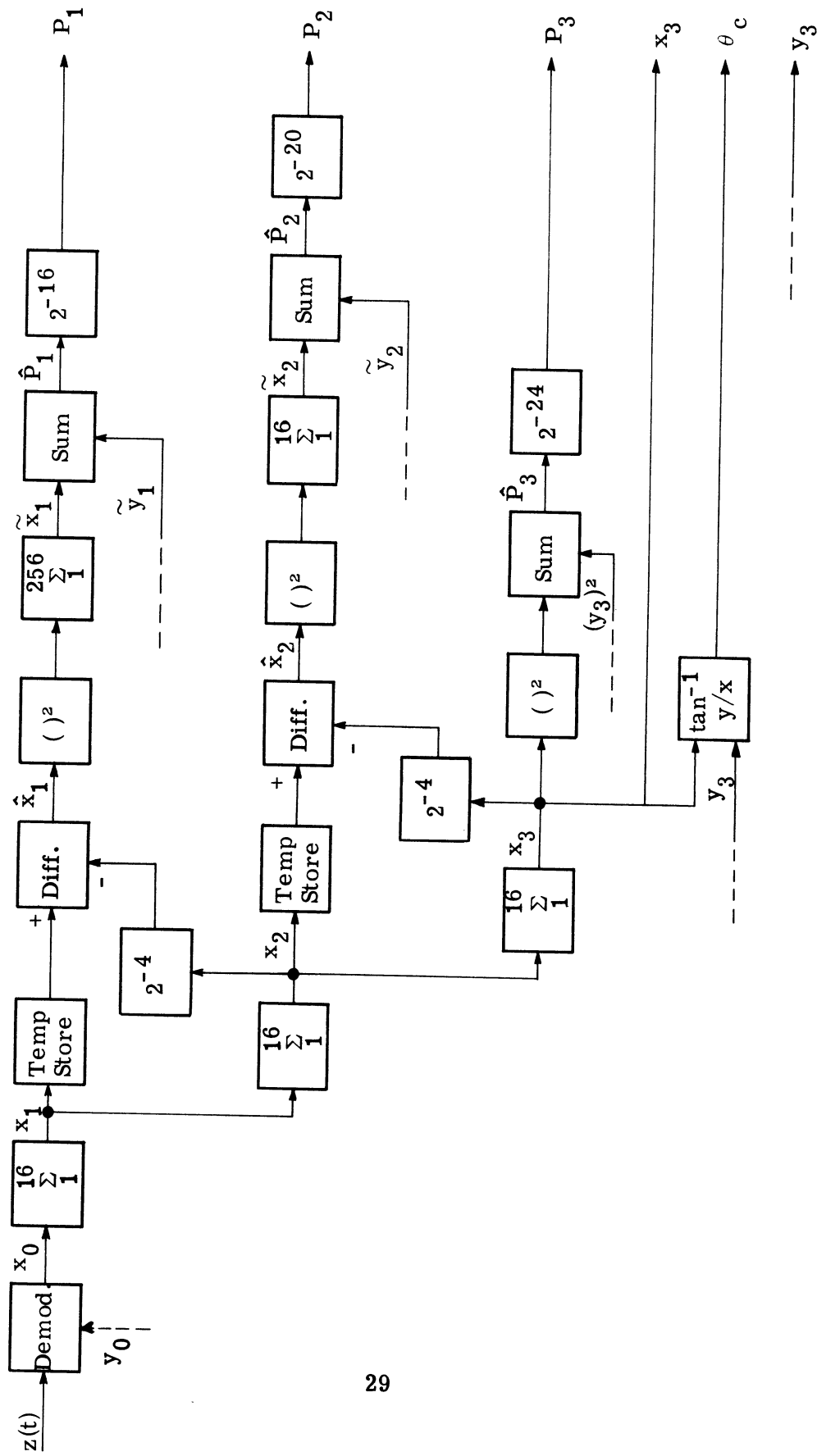
28

Fig. 14. Complete digital process

29

3. RESULTS

This chapter describes the results obtained by the three-filter analysis, summarizes the analysis processes, and discusses an interpretation of these results.

3.1 TRIBAND Graphical Results

In Appendix C the plots of the processed data are presented. Data are presented in frames of approximately seven minutes length; hence, each page represents about two hours of data. Frame #1 started at 1600 hrs., 3 October 1969.

The $\hat{P}_i$ (i = 1, 2, 3) which were stored on magnetic tape were post-processed by a computer program which yielded the plots indicated. The program gives the output in decibels (relative) which is what is actually shown. The scale ranged from a minimum of 10 dB to a maximum of about 68 dB. This range was chosen because the calculated powers never exceeded these limits. In these plots, the following correspondence is used:

(1) $\hat{P}_1 \equiv P(N)$

(2) $\hat{P}_2 \equiv P(I)$

(3) $\hat{P}_3 \equiv P(C)$

Since the phenomena of interest are the relative power levels, the fade occurrences, and the correlation between the three powers, the actual power level is not calculated exactly.

30

results indicate that there are periods of both strong negative and strong positive correlation over each of the time periods used.

3.3 "Phase Jumps" in TRIBAND

The graphical data for the power estimates indicate a strange phenomenon occurring at random intervals. These are the abrupt changes in carrier phase associated with a change in each of the estimated power levels. $\hat{P}_1$ and $\hat{P}_2$ both increase whenever the phase changes while $\hat{P}_3$ (the estimate of the carrier power) decreases.

There appear to be spurious pulses getting into the sample circuitry and causing 90° (or some multiple of 90°) phase jumps during one sample period. These spurious pulses are thought to be caused by a radar transmitter located in the nearby ESSA laboratory.

The phase information for the carrier is given below the three power level plots. The phase angle is expressed as being between -180° and $+180^\circ$ with only -180° being indicated on the plot. The $+180^\circ$ value is understood to be equivalent to the -180° value.

3.2 TRIBAND Correlation Results

The correlation coefficients in power (not in dB) for the three bands was calculated. The relationship used was

$$R_{xy} = \frac{\sum_{i=1}^{N} (x_i - \bar{x})(y_i - \bar{y})}{\left[\sum_{i=1}^{N} (x_i - \bar{x})^2 \sum_{i=1}^{N} (y_i - \bar{y})^2 \right]^{\frac{1}{2}}}$$

where R_{xy} is the correlation coefficient between the sample points $\{x\}$ and $\{y\}$. Also,

$$\bar{x} = \frac{1}{N} \sum_{i=1}^{N} x_i$$

The results are given in Appendix D.

The correlation coefficient was calculated for periods of about 28 minutes and 63 minutes. (That is; $N = 56$ and $N = 126$ with the sample points occurring at 30 second intervals.)

Since this is a nonstationary situation, the correlation coefficient must be viewed as a nonstationary statistic. The calculation

4. CONCLUSION

The initial objectives were met, in that the digital three-band filter was implemented and used to obtain the relative power levels desired. The stability of the phase was again displayed as was evident on previous MIMI CW experiments. This fact tends to establish the validity of the processing.

The carrier power varied from over 60 relative dB (rdB) to about 30 rdB (which occurred during deep fades). This also agrees with the fade situation previously experienced. The local noise level was fairly constant (background noise) with some bursts which may be attributed to biological noise or man-made noise (e.g., shipping). The incoherent power level appeared to be relatively stable, again with the bursts which occur in the local noise band.

As expected, the correlation between the local noise band and the incoherent band is, in general, strongly positive. An interesting observation is that the correlation between the noise band and the coherent band is highly negative on the short time (28 min) basis, and negative to a lesser degree on the longer time calculations. This tends to indicate the presence of higher frequency (> 1 Hz) modulation components which are angle modulating the carrier. To make this definitely conclusive, however, more studies must be carried out.

The digital process described in this report was intended to be a predecessor of an analog process that is to run continuously over a long period of time. When the results of the analog processing are known, the validity of the types and amount of modulation present may be more firmly established.

Appendix A

ON THE QUADRATIC CONTENT TRANSFER FUNCTION

OF A NONLINEAR PROCESSOR

ON THE QUADRATIC CONTENT TRANSFER FUNCTION

OF A NONLINEAR PROCESSOR *

A.1 Background

Consider any time invariant linear filter situation where "the power or energy spectrum" of the input has meaning (Fig. 15). For a steady-state deterministic process, one means a time average; for L_2 deterministic process, one means a time integral; and for a wide sense stationary random process (real or complex), one means the Fourier transform of the autocorrelation.

$$\tilde{x}(t) \quad \boxed{\text{Filter} \quad \begin{array}{c} h(\tau) \\ H(f) \end{array}} \quad x(t)$$
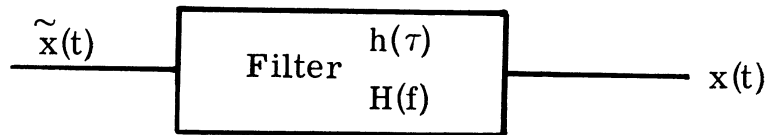
Fig. 15. Filter diagram

One common property of the power or energy spectrum for all these diverse situations is that commonly called Parseval's Theorem.

$$\text{Ave } [x^2(t)] = \int_{-\infty}^{\infty} P_x(f) \, df \tag{1}$$

where $P_x(f)$ is the appropriately defined power or energy spectrum for whatever type of variable x is, and the definition of "Average"

36

---

is the corresponding appropriate time or ensemble average.

A.1.1 Quadratic Content Transfer Function

The power transfer function of a linear time-invariant filter is

$$\text{Power Transfer Function} = |H(f)|^2 \tag{2}$$

where, loosely,

$$H(f) = \mathscr{F}\{\text{impulse response } h(\tau)\} = \mathscr{L}_2\{h(\tau) \text{ at } \mathrm{Re}\ s = 0\}$$

One can relate the average squared output of a linear filter to the input power or energy spectrum and the filter power transfer function by

$$P_x(f) = P_{\underset{x}{\sim}}(f) |H(f)|^2 \tag{3}$$

and

$$\text{Ave}[x^2] = \int_{-\infty}^{\infty} P_{\underset{x}{\sim}}(f) |H(f)|^2 \, df \tag{4}$$

Equation 4 can be used to define a transfer function for both linear and nonlinear processing. Let x be the input to a processor and y be the output. We shall say $T(f|x \rightarrow y)$ is the Quadratic Content transfer function iff

$$\text{Ave } [x^2] \;=\; \int_{-\infty}^{\infty} P_{\widetilde{x}}(f) \; T(f \mid \widetilde{x} \rightarrow x) \; df \tag{5}$$

A.1.2 Quadratic Content Transfer Function of an Average

Consider a finite number of filter outputs and their simple
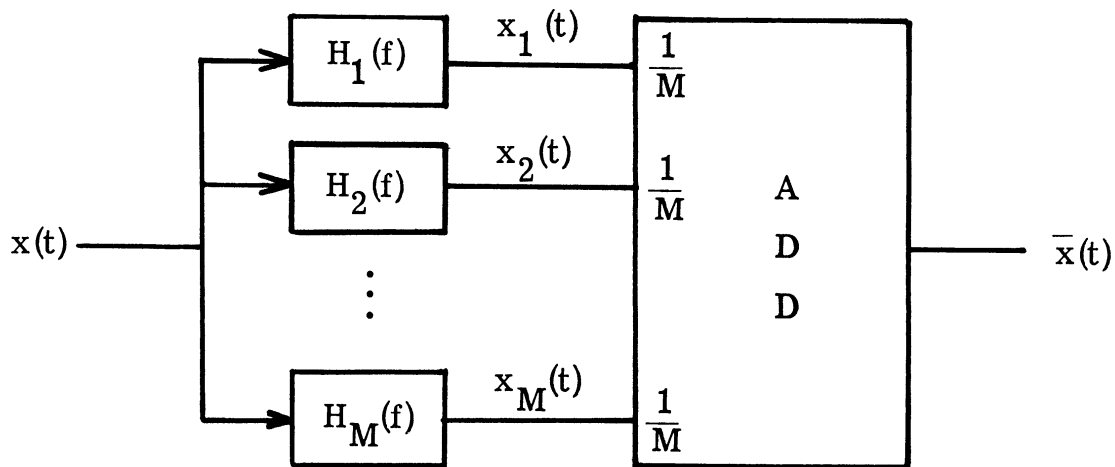
average as diagrammed in Fig. 16.

Fig. 16. Linear averager

$$\overline{x}(t) \;=\; \frac{1}{M} \sum_{k=1}^{M} x_M(t) \tag{6}$$

Because $x \rightarrow x_k \rightarrow \overline{x}$ is a linear processor, we may work directly with

the usual transfer function, and then find its magnitude squared.

$$H(f) \;=\; \frac{1}{M} \sum_{k=1}^{M} H_k(f)$$

$$T(f|x \to \bar{x}) = \left| \frac{1}{M} \sum H_x(f) \right|^2 \qquad (7)$$

Let us not bother to try to simplify Eq. 7.

A.2 RMS Averages

A.2.1 Quadratic Content Transfer Function of an RMS Averager

The first nonlinear processor to be analyzed begins like the simple averager of Fig. 16, with multiple parallel filters. However, instead of the simple average consider the root-mean-square value of the $x_k(t)$.

$$r(t) = \sqrt{\frac{1}{M} \sum_{k=1}^{M} x_k^2(t)} \qquad (8)$$

Here we may not use the usual transfer function, but reason as follows:

$$\text{Ave}[r^2] = \text{Ave} \left[\frac{1}{M} \sum_{k=1}^{M} x_k^2 \right] \qquad (9a)$$

The average of the sum is the sum of the averages.

$$\text{Ave}[r^2] = \frac{1}{M} \sum_{k=1}^{M} \text{Ave}[x_k^2] \qquad (9b)$$

But

$$\text{Ave}\left[x_k^2\right] \;=\; \int_{-\infty}^{\infty} P_{\widetilde{x}}(f)\; |H_k(f)|^2\; df \tag{4}$$

So

$$\text{Ave}\left[r^2\right] \;=\; \frac{1}{M}\sum_{k=1}^{M}\int_{-\infty}^{\infty} P_{\widetilde{x}}(f)\sum_{k}|H_k(f)|^2\; df \tag{9c}$$

$$\text{Ave}\left[r^2\right] \;=\; \int_{-\infty}^{\infty} P_x(f)\left[\frac{1}{M}\sum_{k=1}^{M}|H_k(f)|^2\right]\; df \tag{9d}$$

Thus

$$T(f\,|\,x\to r) \;=\; \frac{1}{M}\sum_{k=1}^{M}|H_k(f)|^2 \tag{10}$$

A.2.2 Quadratic Content Transfer Function of the RMS About the Average

The second nonlinear processor again begins like the previous one, with $x(t)$ filtered to yield the set $\{x_k(t)\}$. Equation 6 still defines $\bar{x}(t)$. However, let $s(t)$ be

$$s(t) \;=\; \sqrt{\frac{1}{M}\sum_{k=1}^{M}\left(x_k(t) - \bar{x}(t)\right)^2} \tag{11}$$

$$s^2 \;=\; \frac{1}{M}\sum\left(x_k^2 - 2\bar{x}x_k + \bar{x}^2\right) \tag{12a}$$

$$s^2 \;=\; \frac{1}{M}\sum x_k^2 - 2\bar{x}\left(\frac{1}{M}\sum x_k\right) + \bar{x}^2 \tag{12b}$$

$$s^2 = r^2 - 2\bar{x}\bar{x} + \bar{x}^2 = r^2 - \bar{x}^2 \qquad (12c)$$

$$s^2(t) = r^2(t) - \bar{x}^2(t) \qquad (12d)$$

Again using the linearity of average

$$\mathrm{Ave}[s^2(t)] = \mathrm{Ave}[r^2(t)] - \mathrm{Ave}[\bar{x}^2(t)] \qquad (13)$$

and the linearity of the integral over frequency yields

$$T(f|x \to s) = T(f|x \to r) - T(f|x \to \bar{x}) \qquad (14)$$

Gathering together (7) and (10) yields

$$T(f|x \to s) = \frac{1}{M} \sum |H_k(f)|^2 - \left|\frac{1}{M} \sum H_k(f)\right|^2 \qquad (15)$$

A.3 Delay Lines and Averages

A.3.1 General Delays

In this section we shall consider the case when the parallel filters are pure delay functions.

$$h_k(\tau) = \delta(\tau - \tau_k) \qquad H_k(f) = e^{-j2\pi f \tau_k} \qquad (16)$$

$$T(f|x \to \bar{x}) = \left|\frac{1}{M} \sum_{k=1}^{M} e^{-j2\pi f \tau_k}\right|^2 \qquad (17)$$

41

$$T(f|x \rightarrow r) = \frac{1}{M} \sum_{k=1}^{M} \left| e^{-j2\pi f \tau_k} \right|^2 = 1 \qquad (18)$$

$$T(f|x \rightarrow s) = 1 - T(f|x \rightarrow \bar{x}) \qquad (19)$$

Apparently the rms averager, (18), is the only nice result.

A.3.2 Uniformly Spaced Delays

Let us consider

$$\tau_k = k \Delta + \tau_0 \qquad (20)$$

The corresponding filters are realizable iff $\tau_1 = \Delta + \tau_0 \geq 0$. From experience we learn to factor the exponent

$$-j 2\pi f(k\Delta + \tau_0) = -j\pi f(M\Delta + \Delta + 2\tau_0) - j\pi f(2k - 1 - M) \Delta \qquad (21)$$

$$\frac{1}{M} \sum_{k=1}^{M} H_k(f) = \exp\left(-j\pi f(M\Delta + \Delta + 2\tau_0) \right)$$

$$\frac{1}{M} \sum_{k=1}^{M} \exp\left(-j\pi f(2k - 1 - M) \Delta \right) \qquad (22)$$

The sum is the sum of a finite geometric series, with ratio between terms of $\exp(-j\pi f 2\Delta)$. Its sum is

$$\sum_{k=1}^{M} \exp(---) = \frac{e^{-j\pi f(1 - M)\Delta} - e^{-j\pi f(M + 1)\Delta}}{1 - e^{-j\pi f 2\Delta}} \qquad (23a)$$

42

Factoring out $e^{-j\pi f\Delta}$ from every term

$$= \frac{e^{-j\pi f(-M)\Delta} - e^{-j\pi fM\Delta}}{e^{j\pi f\Delta} - e^{-j\pi f\Delta}} \tag{23b}$$

$$= \frac{\sin \pi M f \Delta}{\sin \pi f \Delta} \tag{23c}$$

Returning to Eq. 22,

$$\frac{1}{M} \sum_{k=1}^{M} H_k(f) = \exp\left(-j\pi f(M\Delta + \Delta + \tau_0)\right) \frac{\sin \pi M f \Delta}{M \sin \pi f \Delta} \tag{24}$$

The first factor represents the average delay of $\tau_0 + .5(M+1)$; and has unity magnitude. The second factor is real; it is the periodic analog of the sinc function

$$\text{sinc}(fT) = \frac{\sin \pi fT}{\pi fT} \tag{25}$$

The rest is a quick summary

$$T(f|x \rightarrow \bar{x}) = \left[\frac{\sin \pi M f \Delta}{M \sin \pi f \Delta}\right]^2 \tag{26}$$

$$T(f|x \rightarrow r) = 1 \tag{27}$$

$$T(f|x \rightarrow s) = 1 - \left[\frac{\sin \pi M f \Delta}{M \sin \pi f \Delta}\right]^2 \tag{28}$$

A.4 Analog Triband Using Uniform Delay

The subprograms in the digital triband processor use all three kinds of average discussed above (simple, rms, and standard deviation) and also use analog filtering between the raw inputs and the computer, and a demodulation process through synchronous sampling.

In this section I should like to consider an analog analogy to that processing that occurs after the input filtering and demodulation. We know that these yield a complex signal that is physically limited to low frequencies, and that only values at discrete instants of time are available because of the sampling. In this analogy I shall suppress these features until late in the analysis.

The processing is block diagrammed in Fig. 17.
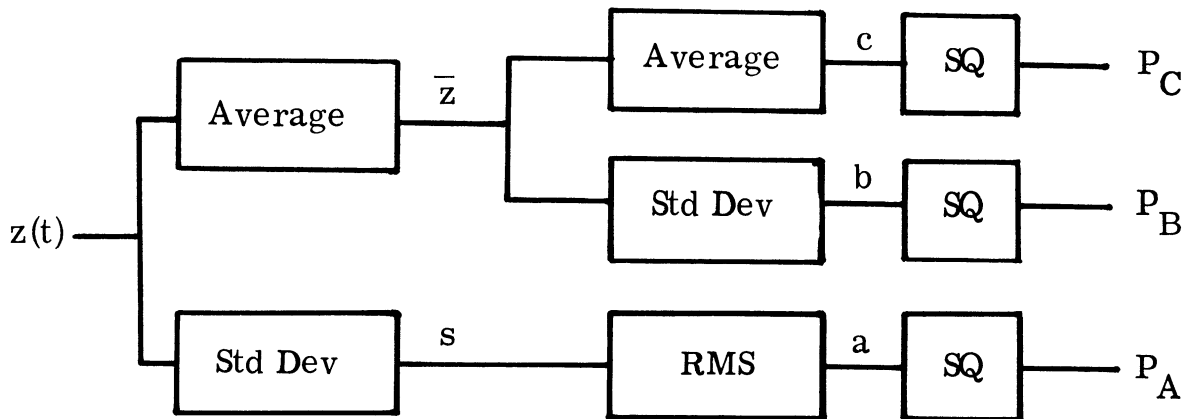
Fig. 17. Triband post demodulation processing

What is desired is the Quadratic Content Transfer Characteristics between $z(t)$ and $a(t)$, $b(t)$, and $c(t)$. If the input power (energy) spectrum $P_z(f)$ is known, then the Quadratic Content Transfers could be used to obtain $\text{Ave}[P_A]$, $\text{Ave}[P_B]$, and $\text{Ave}[P_C]$.

The first average and standard deviation processors use M_1 values each, and the time separation is T_1

$$T(f \mid z \to \bar{z}) = \left(\frac{\sin \pi M_1 T_1 f}{M_1 \sin \pi T_1 f} \right)^2 \tag{29}$$

$$T(f \mid z \to s) = 1 - \left(\frac{\sin \pi M_1 T_1 f}{M_1 \sin \pi T_1 f} \right)^2 \tag{30}$$

The second layer of processors use M_2 values, and the time separation is $T_2 = M_1 T_1$

$$T(f \mid \bar{z} \to c) = \left(\frac{\sin \pi M_2 M_1 T_1 f}{M_2 \sin \pi M_1 T_1 f} \right)^2 \tag{31}$$

$$T(f \mid \bar{z} \to b) = 1 - \left(\frac{\sin \pi M_1 M_2 T_1 f}{M_2 \sin \pi M_1 T_1 f} \right)^2 \tag{32}$$

$$T(f \mid s \to a) = 1 \tag{33}$$

The Quadratic Content transfer function of a cascade of these processors is the product of the individual Quadratic Content transfer functions.

45

Hence

$$T(f \mid z \rightarrow c) = T(f \mid z \rightarrow \bar{z}) \, T(f \mid \bar{z} \rightarrow c) \tag{34a}$$

$$T(f \mid z \rightarrow c) = \left(\frac{\sin \pi \, M_2 M_1 T_1 \, f}{M_1 M_2 \, \sin \pi \, T_1 \, f} \right)^2 \tag{34b}$$

$$T(f \mid z \rightarrow b) = T(f \mid z \rightarrow \bar{z}) \, T(f \mid \bar{z} \rightarrow b) \tag{35a}$$

$$T(f \mid z \rightarrow b) = \left(\frac{\sin \pi \, M_1 T_1 \, f}{M_1 \, \sin \pi \, T_1 \, f} \right)^2 - \left(\frac{\sin \pi \, M_1 M_2 T_1 \, f}{M_1 M_2 \, \sin \pi \, T_1 \, f} \right)^2 \tag{35b}$$

$$T(f \mid z \rightarrow a) = T(f \mid z \rightarrow s) \, T(f \mid s \rightarrow a) \tag{36a}$$

$$T(f \mid z \rightarrow a) = 1 - \left(\frac{\sin \pi \, M_1 T_1 \, f}{M_1 \, \sin \pi \, T_1 \, f} \right)^2 \tag{36b}$$

Because the sum of these three transfer functions is unity

$$T(f \mid z \rightarrow a) + T(f \mid z \rightarrow b) + T(f \mid z \rightarrow c) = 1 \tag{37}$$

we call these three "complementary," that is, "all the input power is split, and gets through so none is lost or reflected."

Equations 34, 35, and 36 are the basic equations used in understanding the special features of TRIBAND. They are repeated below for $M_1 = M_2 = 16$ and $T_1 = \frac{8}{105}$. Let $f_1 = \frac{105}{8} = 13.125$ Hz

46

$$T(f \mid z \to c) = \left(\frac{\sin \pi \; 256 \; f/f_1}{256 \; \sin \pi \; f/f_1} \right)^2 \tag{34c}$$

$$T(f \mid z \to b) = \left(\frac{\sin \pi \; 16 \; f/f_1}{16 \; \sin \pi \; f/f_1} \right)^2 - \left(\frac{\sin \pi \; 256 \; f/f_1}{256 \; \sin \pi \; f/f_1} \right)^2 \tag{35c}$$

$$T(f \mid z \to a) = 1 - \left(\frac{\sin \; 16 \; f/f_1}{16 \; \sin \pi \; f/f_1} \right)^2 \tag{36c}$$

All of these transfer functions are periodic, with period 13.125 Hz. The carrier band, "C band," is centered at 0 Hz and has first zeros at $\pm .051^+$ Hz. The first sideband, "B band," first nears unity transfer at .051 Hz, and has its first zero (other than 0 Hz) at $\pm .820^+$ Hz. The "A band" first approaches unity transfer at $\pm .820$ Hz, and has its first zero (other than at 0 Hz) at ± 13.125 Hz. The crossover frequencies are $f_{CB} = \pm .026$ Hz, $f_{BA} = \pm .410$ Hz.

Appendix B

INDIVIDUAL POWER TRANSFER CHARACTERISTIC

PLOTS

$$1 + \left[\frac{\sin(\pi 16 f\tau)}{16\sin(\pi f\tau)}\right]^2 - 2\,\frac{\sin(\pi 16 f\tau)}{16\sin(\pi f\tau)}\,\cos(15-2k)\,\pi f\tau$$
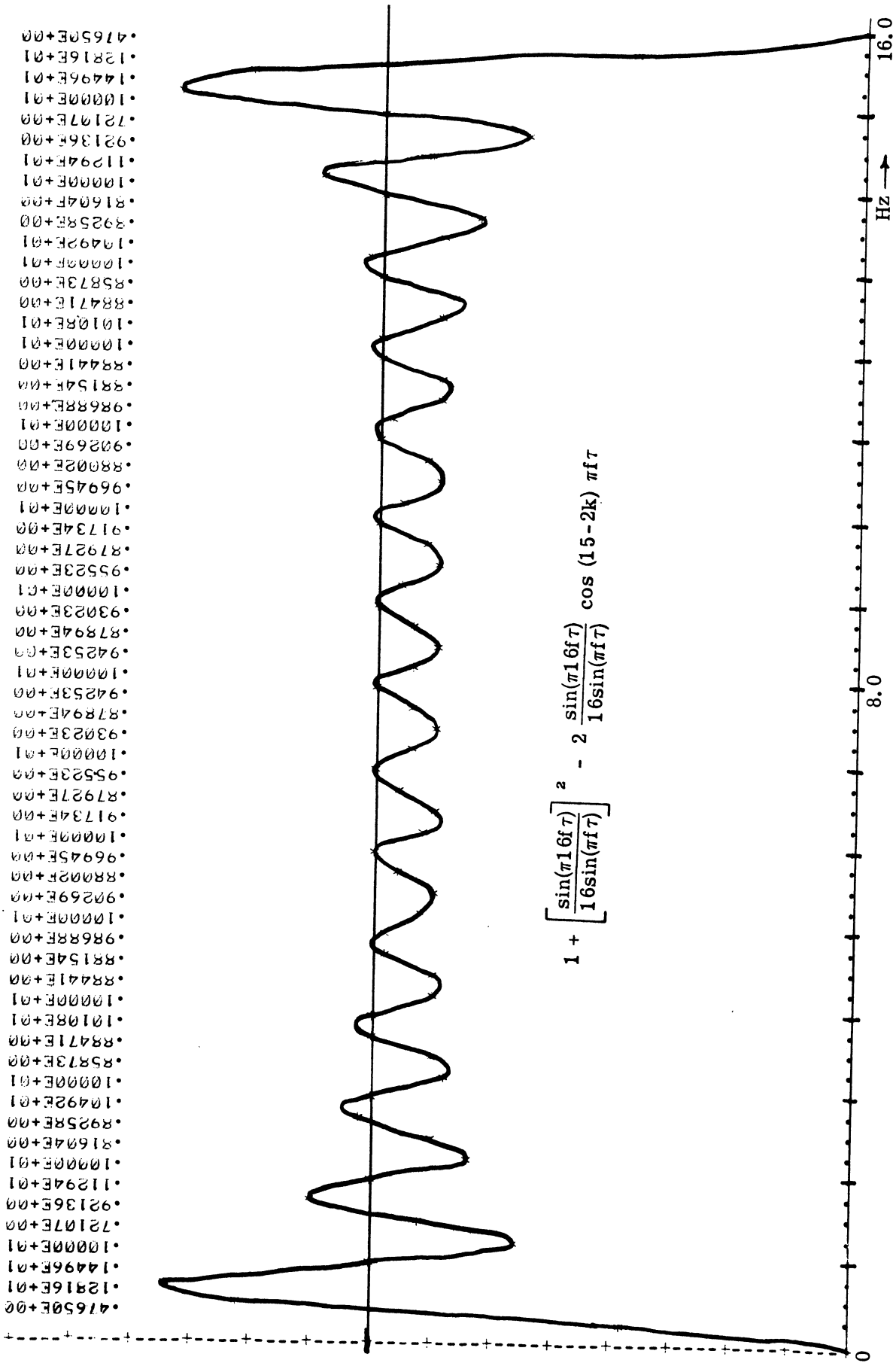
Fig. 18. Individual power transfer characteristic, k = 0, 15

$$1 + \left[\frac{\sin(\pi 16 f\tau)}{16\sin(\pi f\tau)}\right]^2 - 2\,\frac{\sin(\pi 16 f\tau)}{16\sin(\pi f\tau)}\cos(15-2k)\,\pi f\tau$$

Hz ⟶

0   8.0   16.0
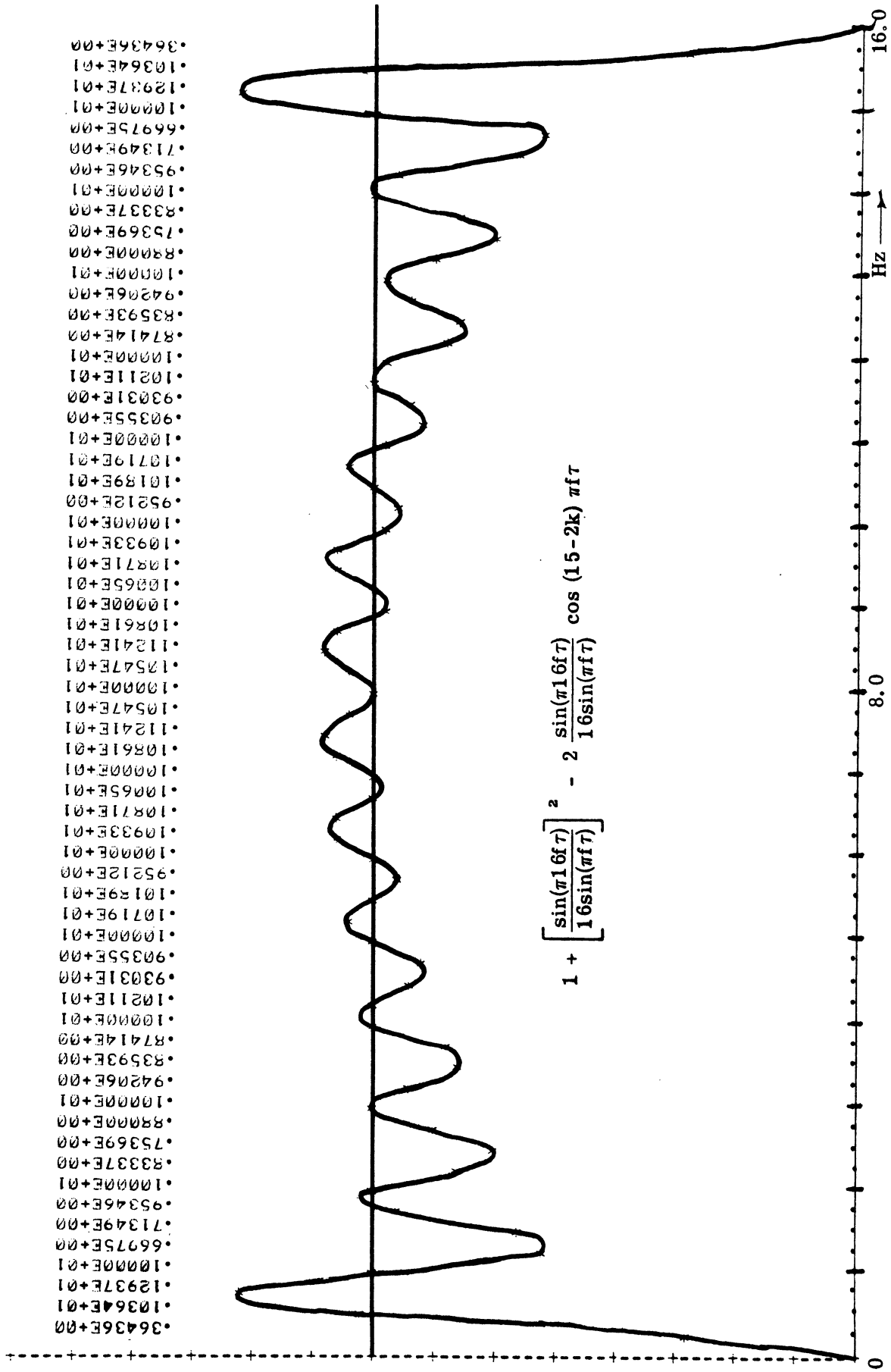
Fig. 19. Individual power transfer characteristic, k = 1,14

$$1 + \left[\frac{\sin(\pi 16 f \tau)}{16 \sin(\pi f \tau)}\right]^{2} - 2 \frac{\sin(\pi 16 f \tau)}{16 \sin(\pi f \tau)} \cos(15 - 2k) \pi f \tau$$

Fig. 20. Individual power transfer characteristic, k = 2, 13

51

$$1 + \left[\frac{\sin(\pi 16 f\tau)}{16\sin(\pi f\tau)}\right]^{2} - 2\,\frac{\sin(\pi 16 f\tau)}{16\sin(\pi f\tau)}\,\cos(15-2k)\,\pi f\tau$$

Hz →

0   8.0   16.0

Fig. 21.   Individual power transfer characteristic, k = 3, 12

$$1 + \left[\frac{\sin(\pi 16 f\tau)}{16\sin(\pi f\tau)}\right]^2 - 2\,\frac{\sin(\pi 16 f\tau)}{16\sin(\pi f\tau)}\cos(15-2k)\,\pi f\tau$$
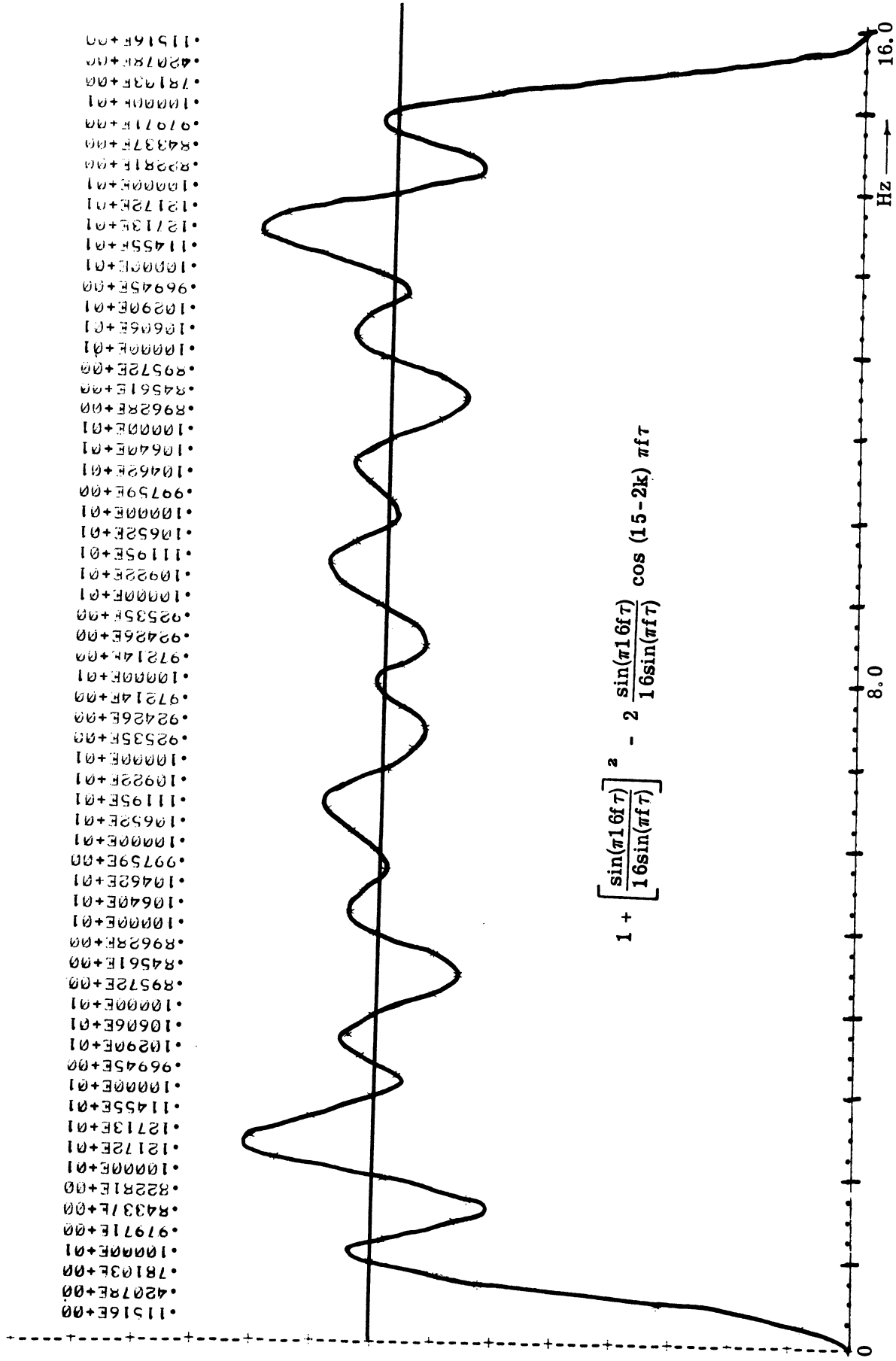
Fig. 22. Individual power transfer characteristic, k = 4,11

Hz ⟶

0   8.0   16.0

53

$$1 + \left[\frac{\sin(\pi 16f\tau)}{16\sin(\pi f\tau)}\right]^2 - 2\,\frac{\sin(\pi 16f\tau)}{16\sin(\pi f\tau)}\cos(15-2k)\,\pi f\tau$$

Hz ⟶

0   8.0   16.0
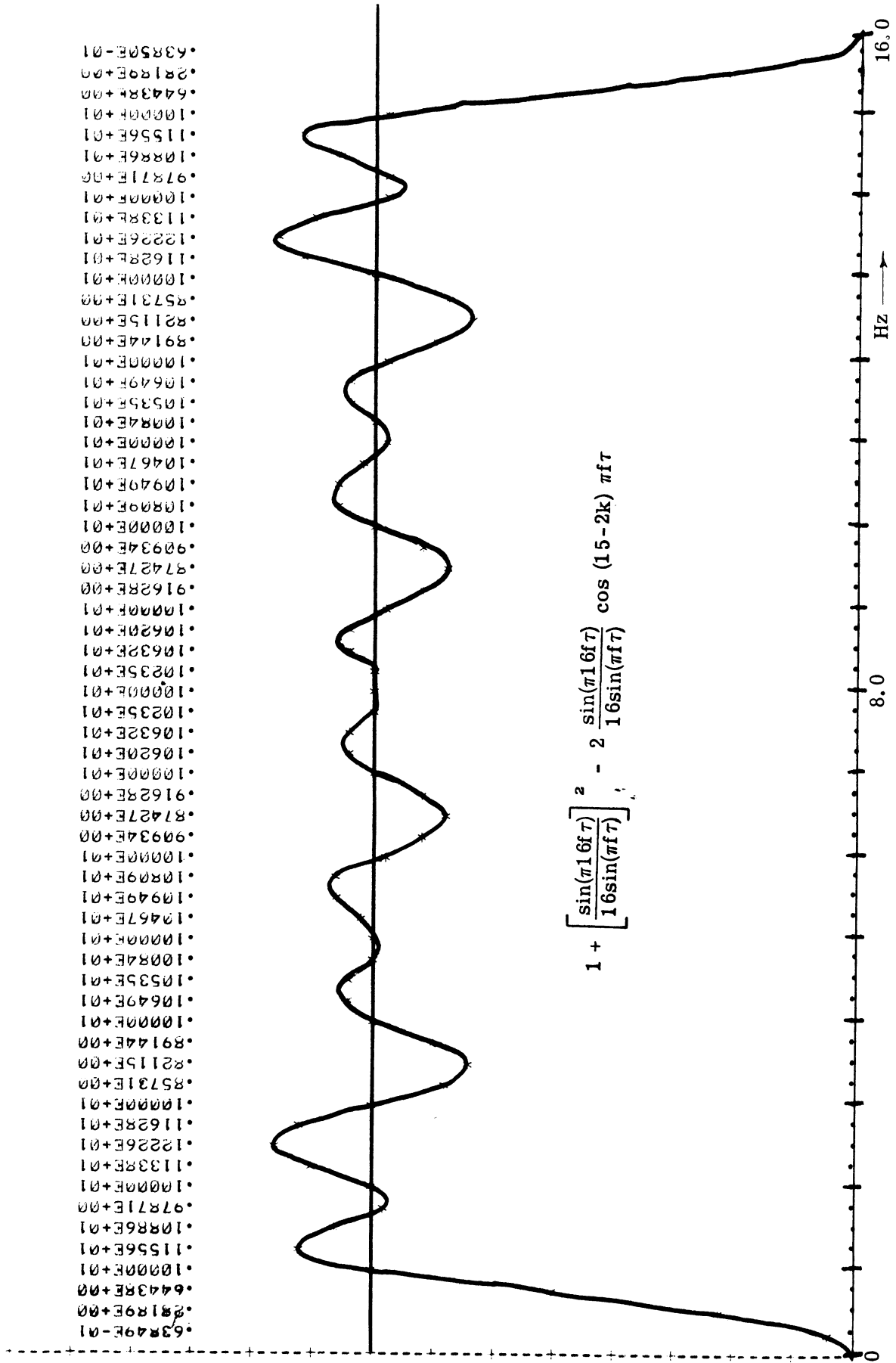
Fig. 23.   Individual power transfer characteristic, k = 5, 10

$$1 + \left[\frac{\sin(\pi 16 f\tau)}{16\sin(\pi f\tau)}\right]^2 - 2\,\frac{\sin(\pi 16 f\tau)}{16\sin(\pi f\tau)}\cos(15-2k)\,\pi f\tau$$

Fig. 24. Individual power transfer characteristic, k = 6, 9
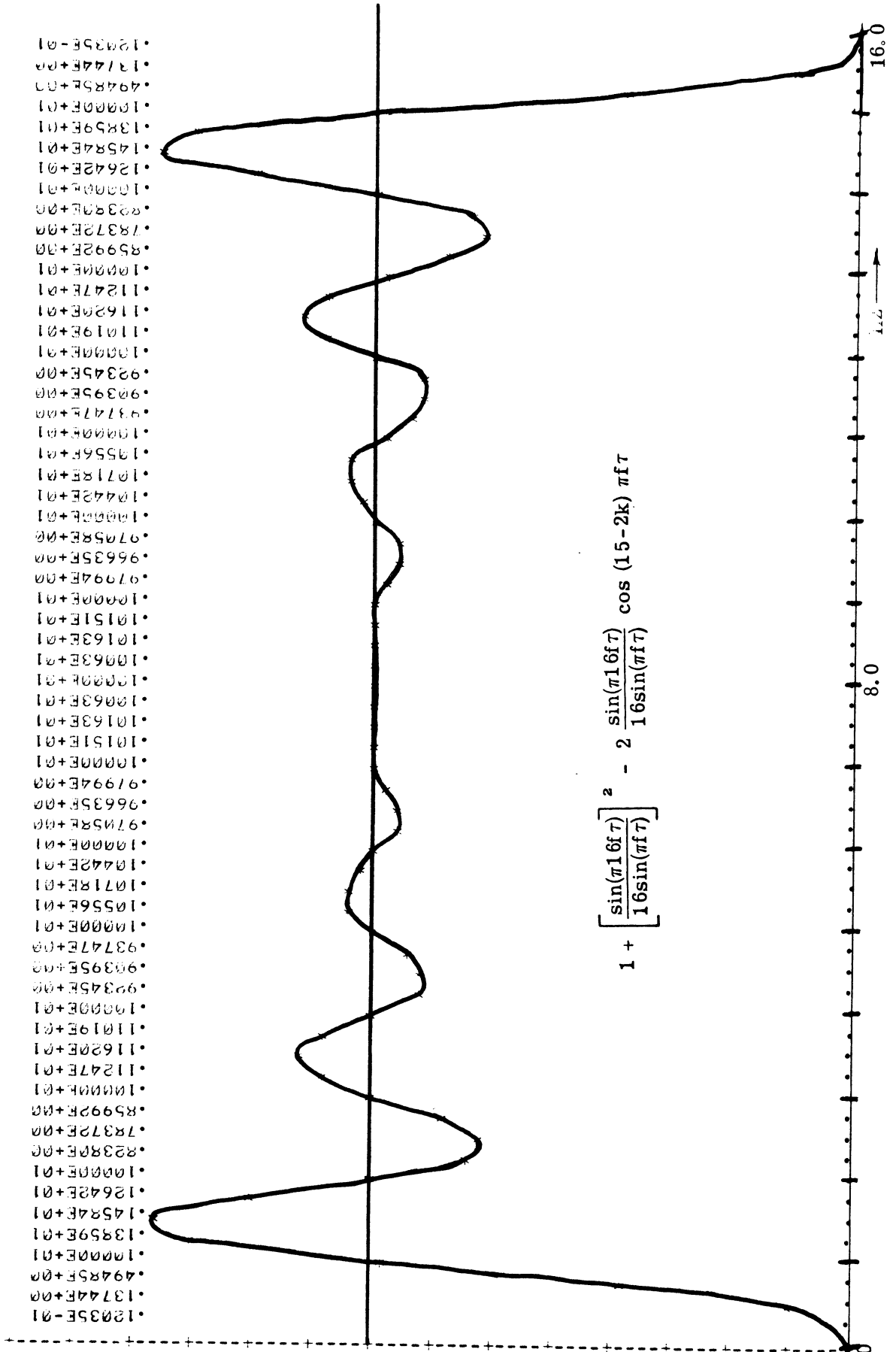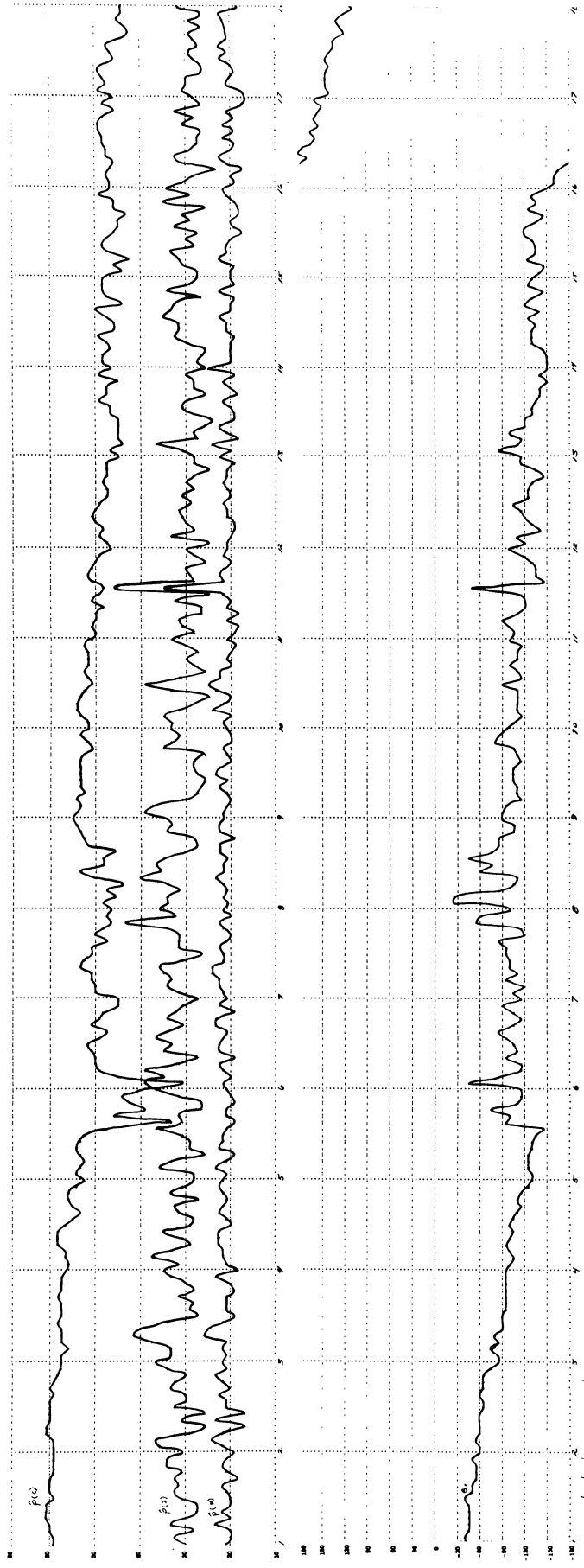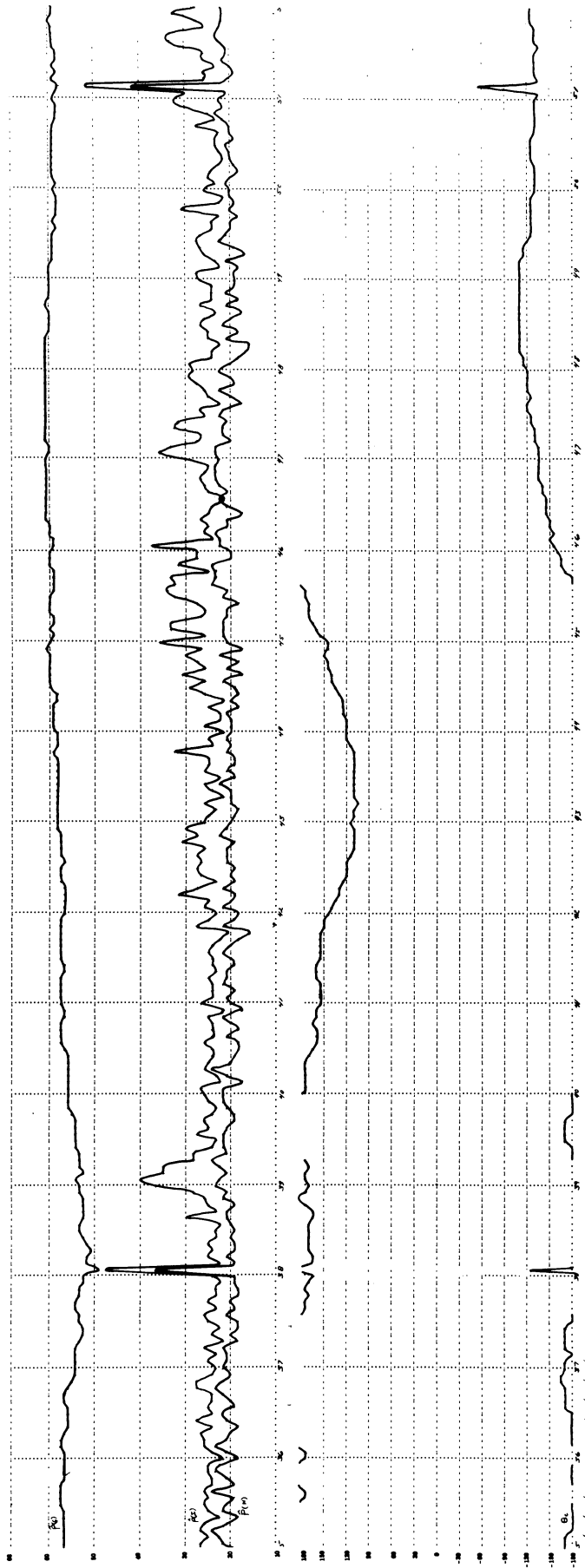
Fig. 25. Individual power transfer characteristic, k = 7, 8

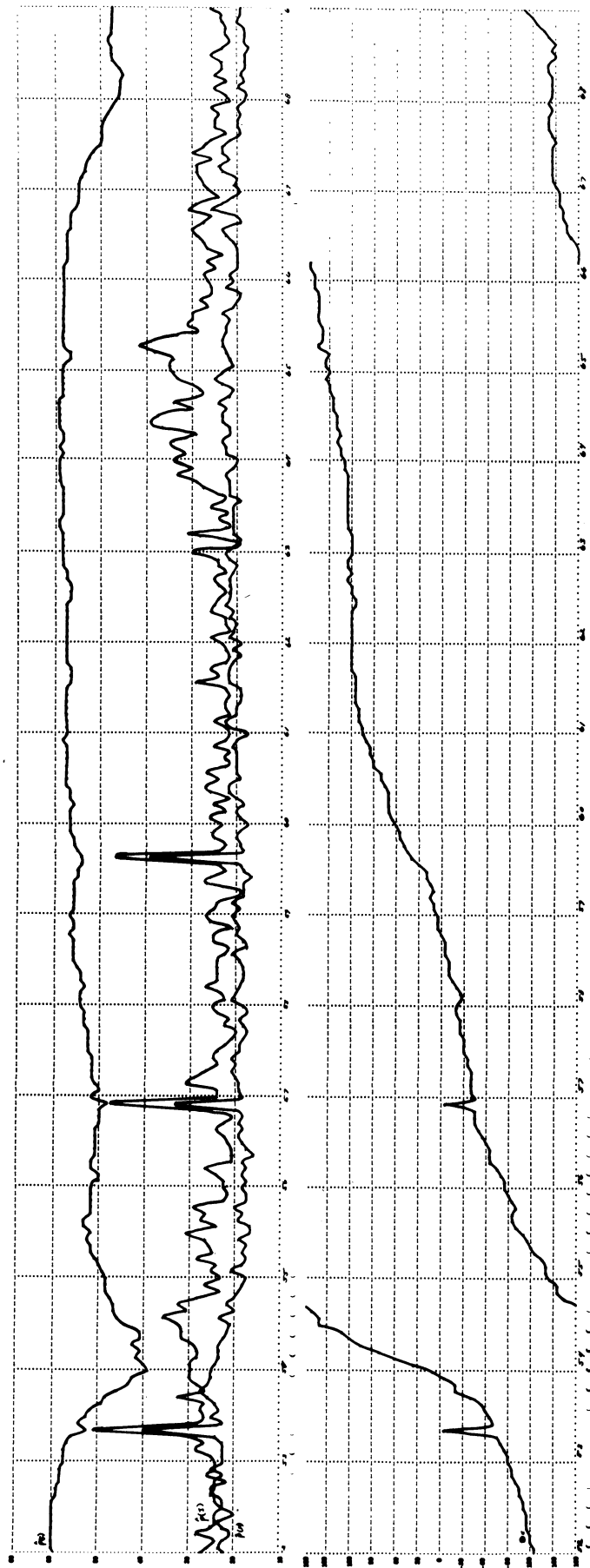$$1 + \left[\frac{\sin(\pi 16 f\tau)}{16\sin(\pi f\tau)}\right]^2 - 2\,\frac{\sin(\pi 16 f\tau)}{16\sin(\pi f\tau)}\cos(15-2k)\,\pi f\tau$$

Appendix C

TRIBAND GRAPHICAL RESULTS

67

69

70

73
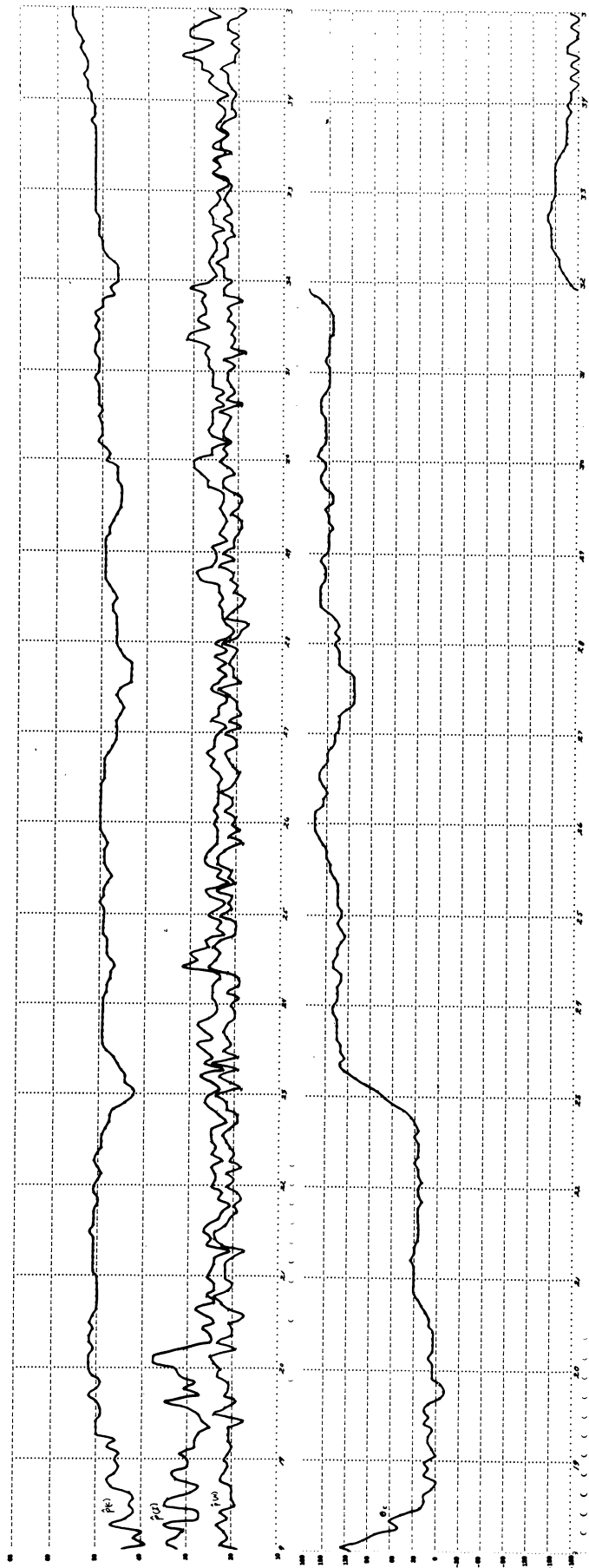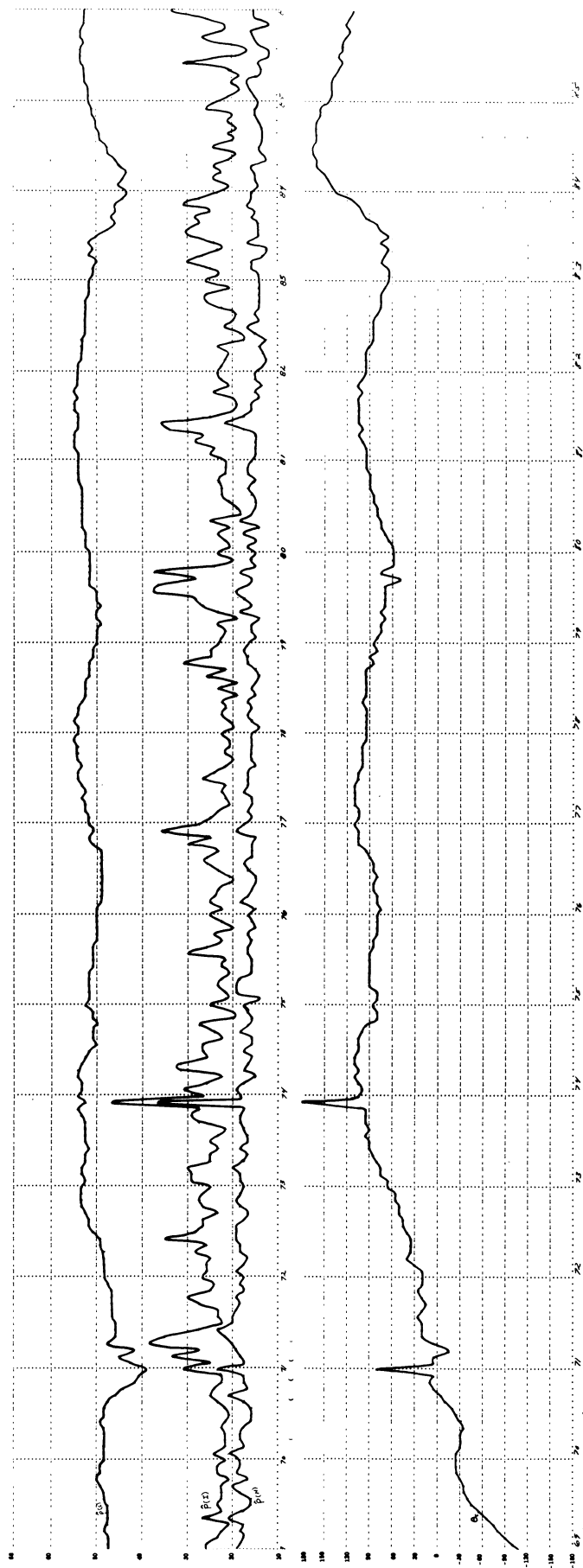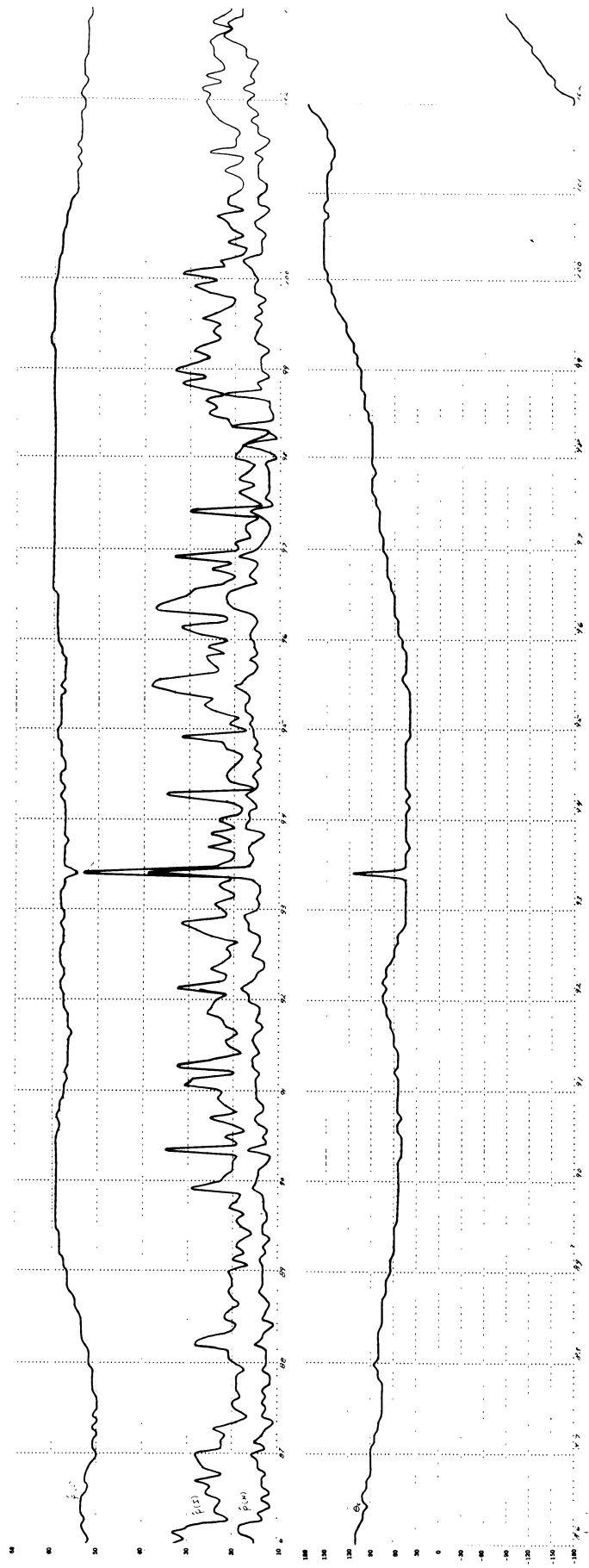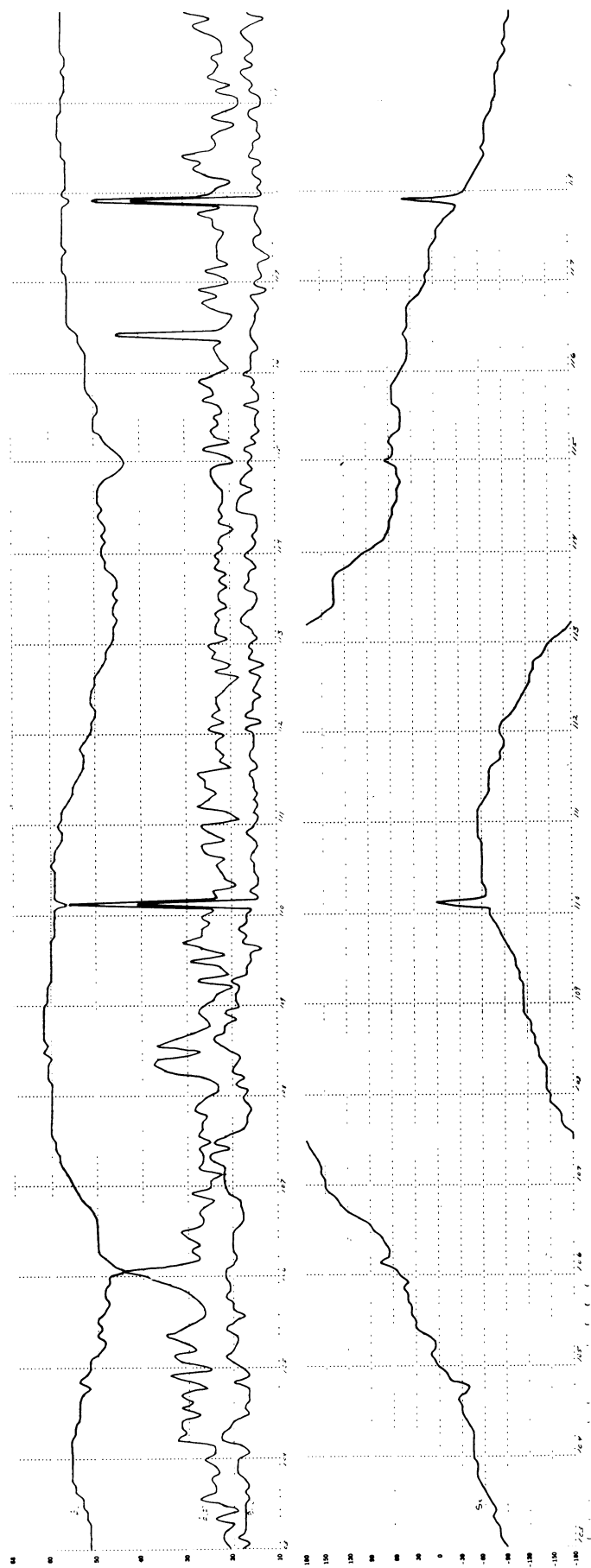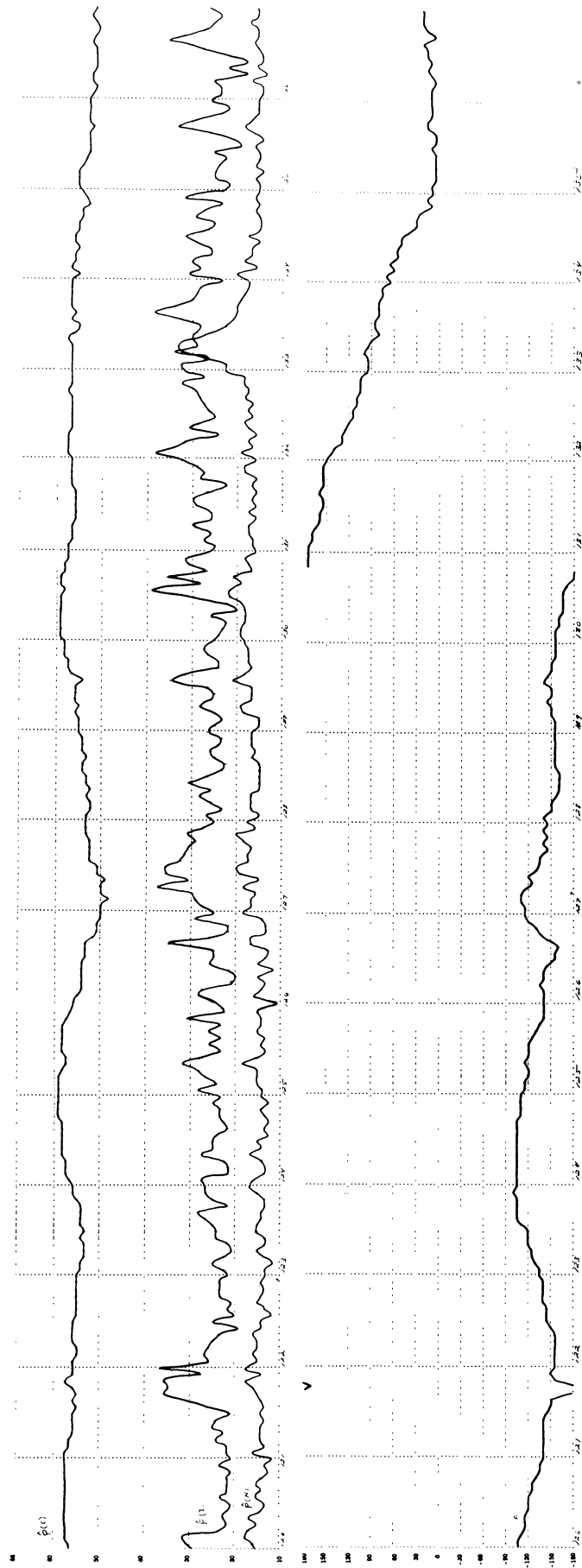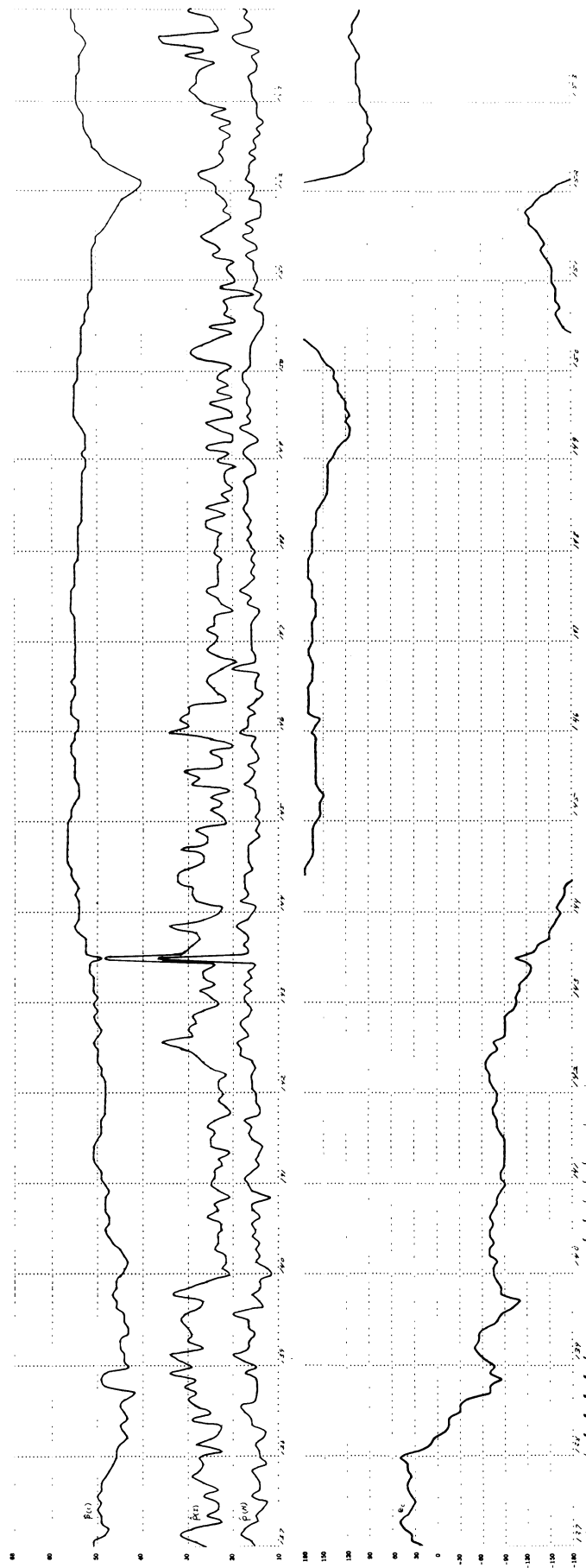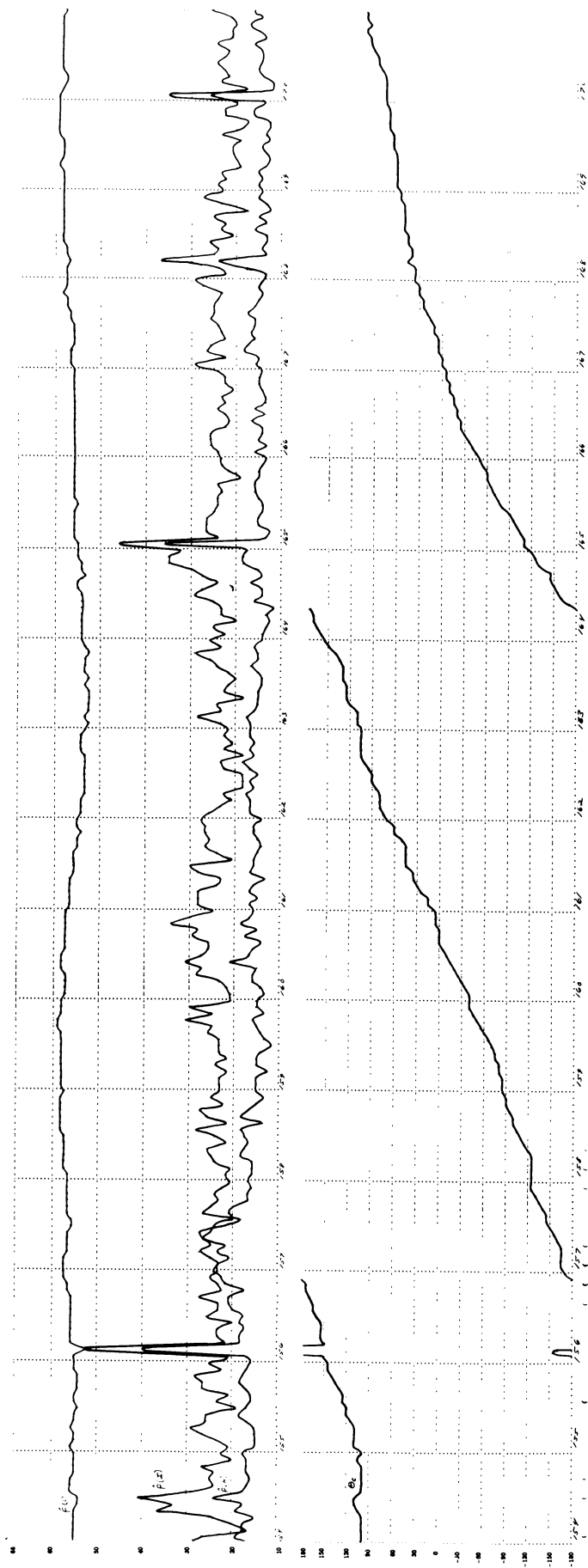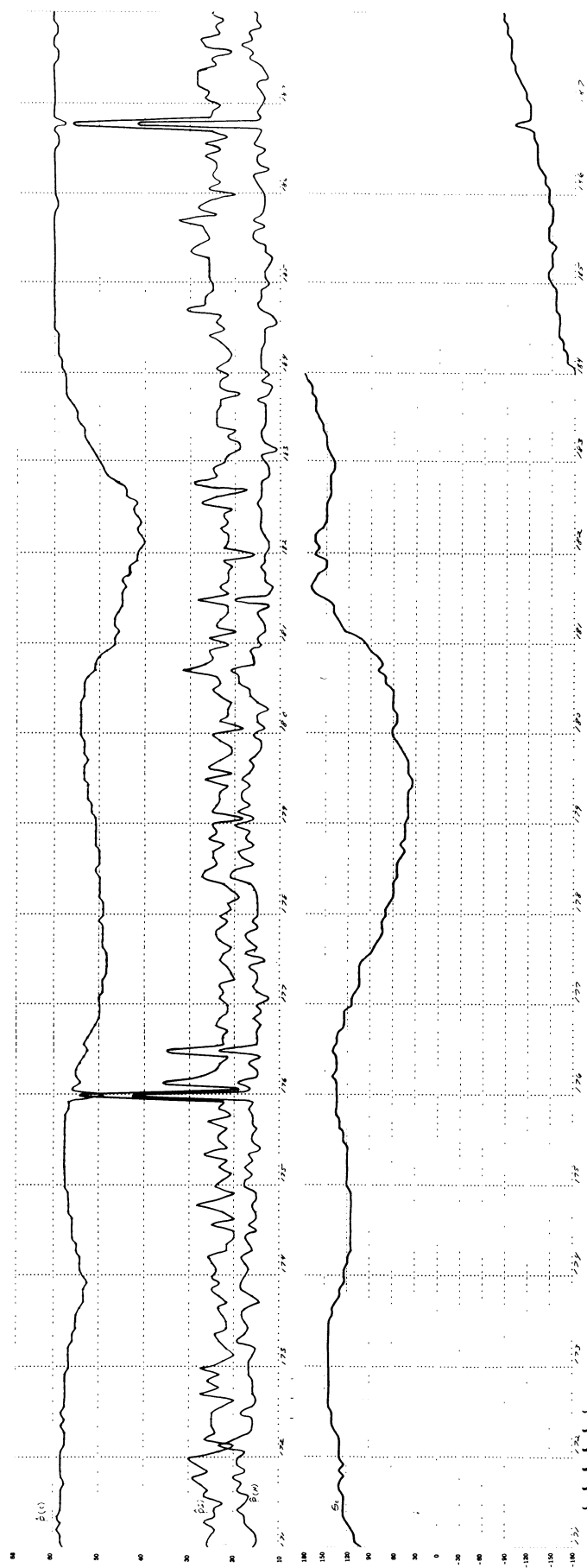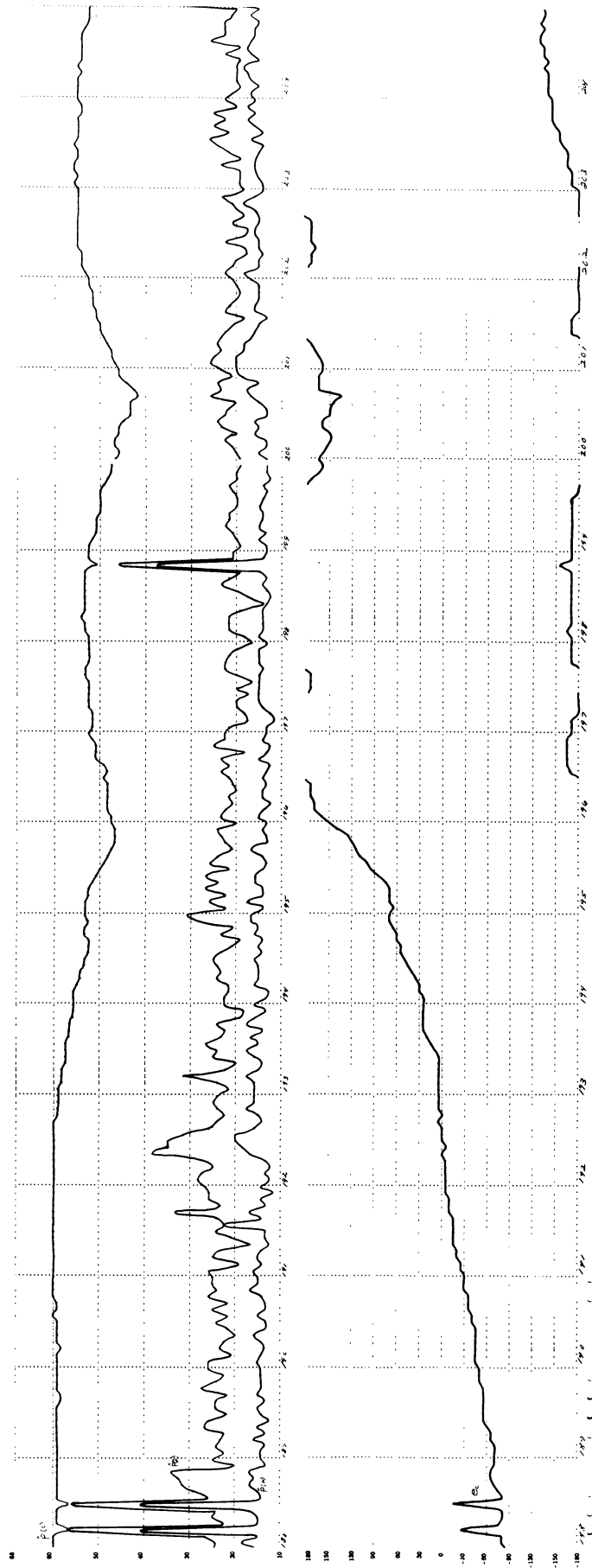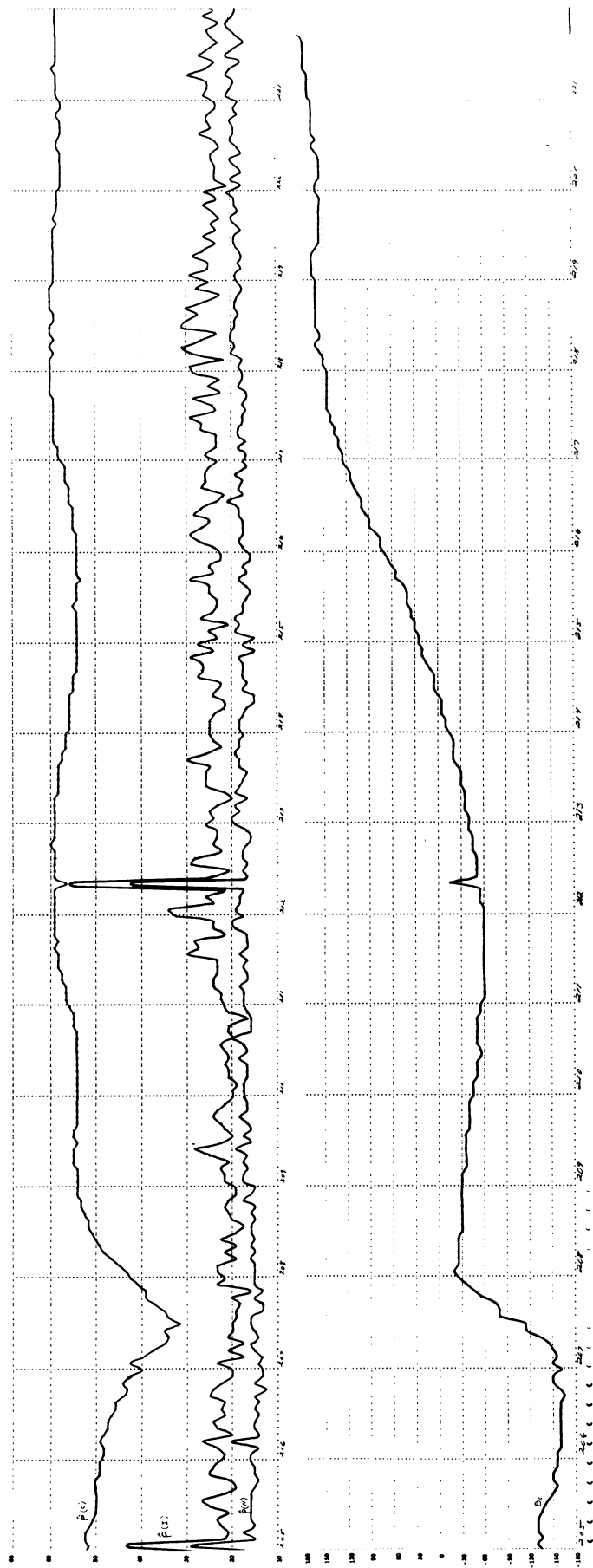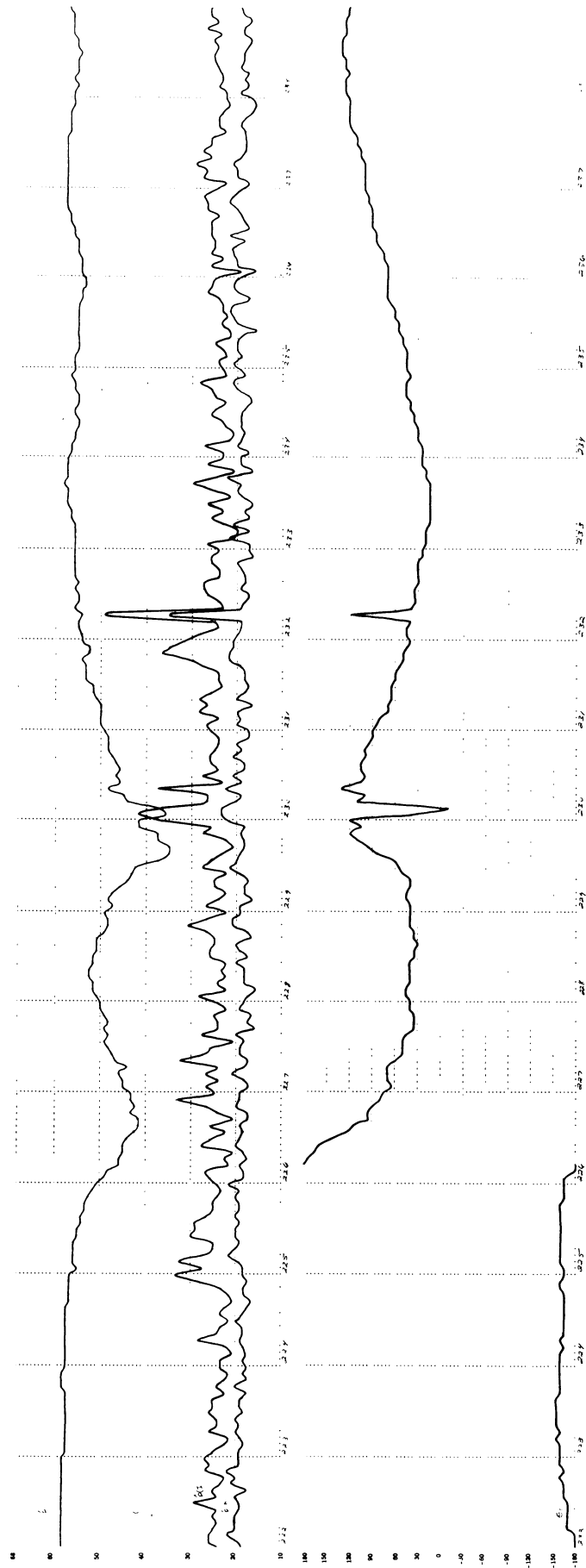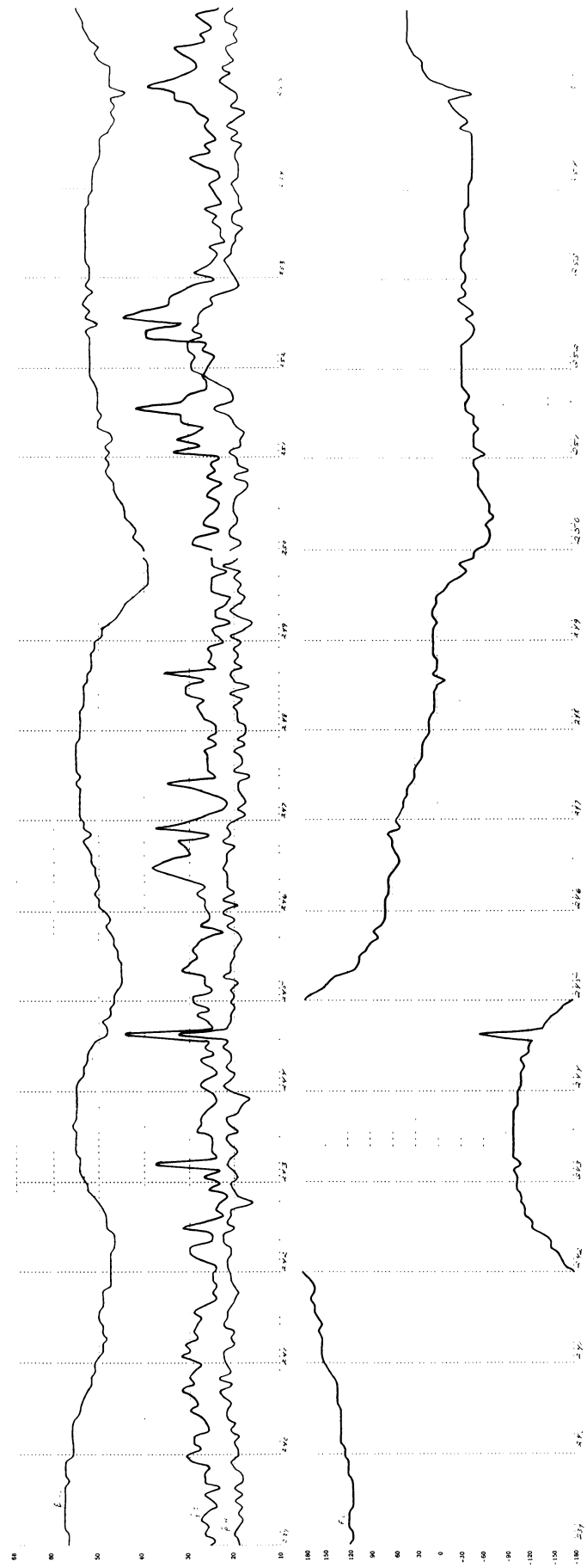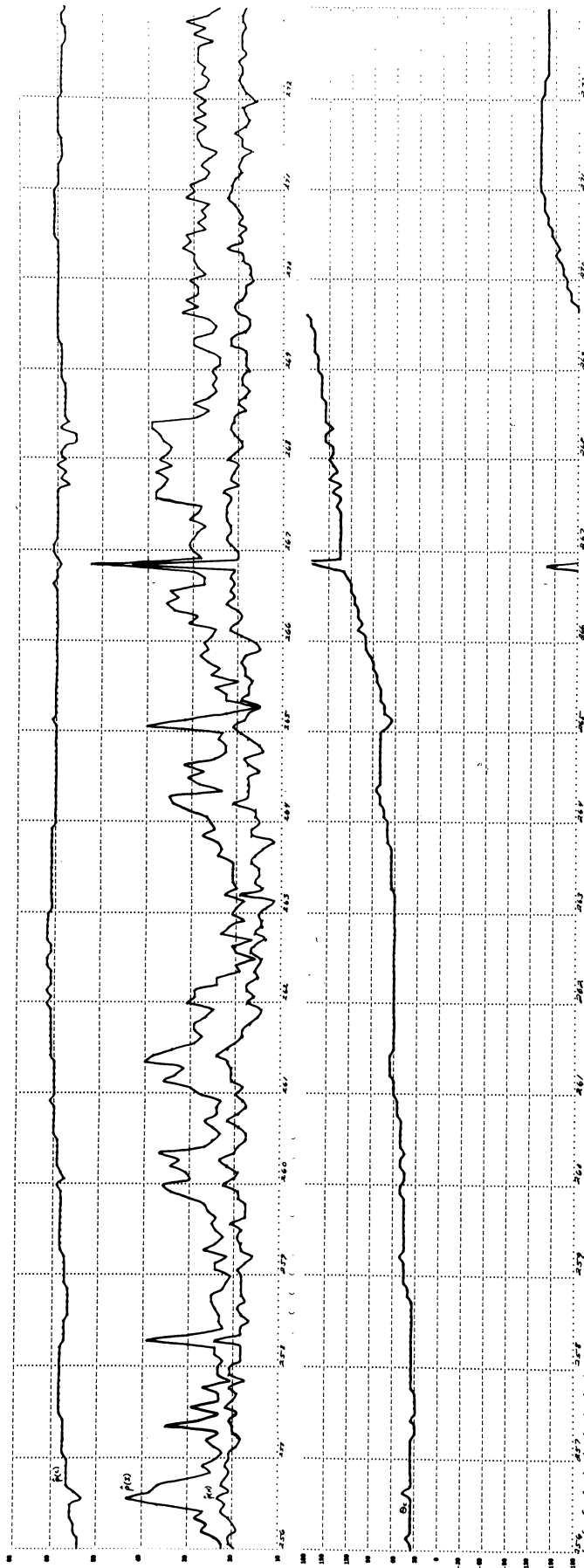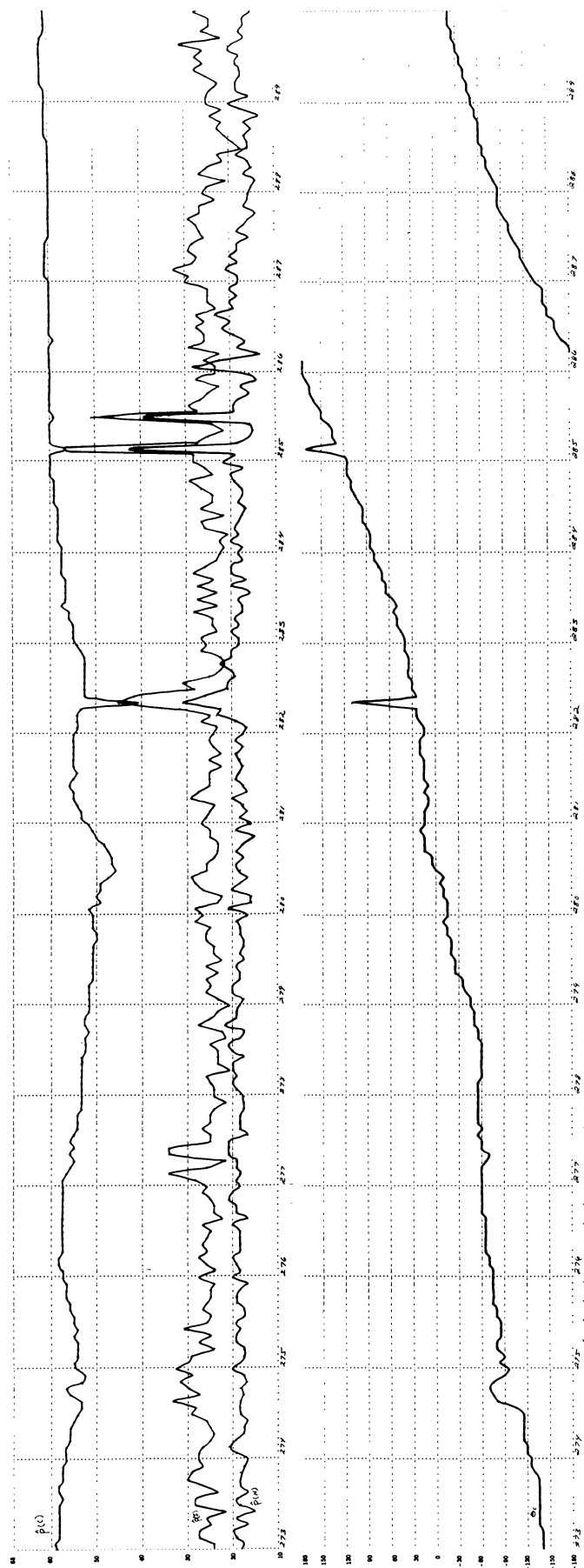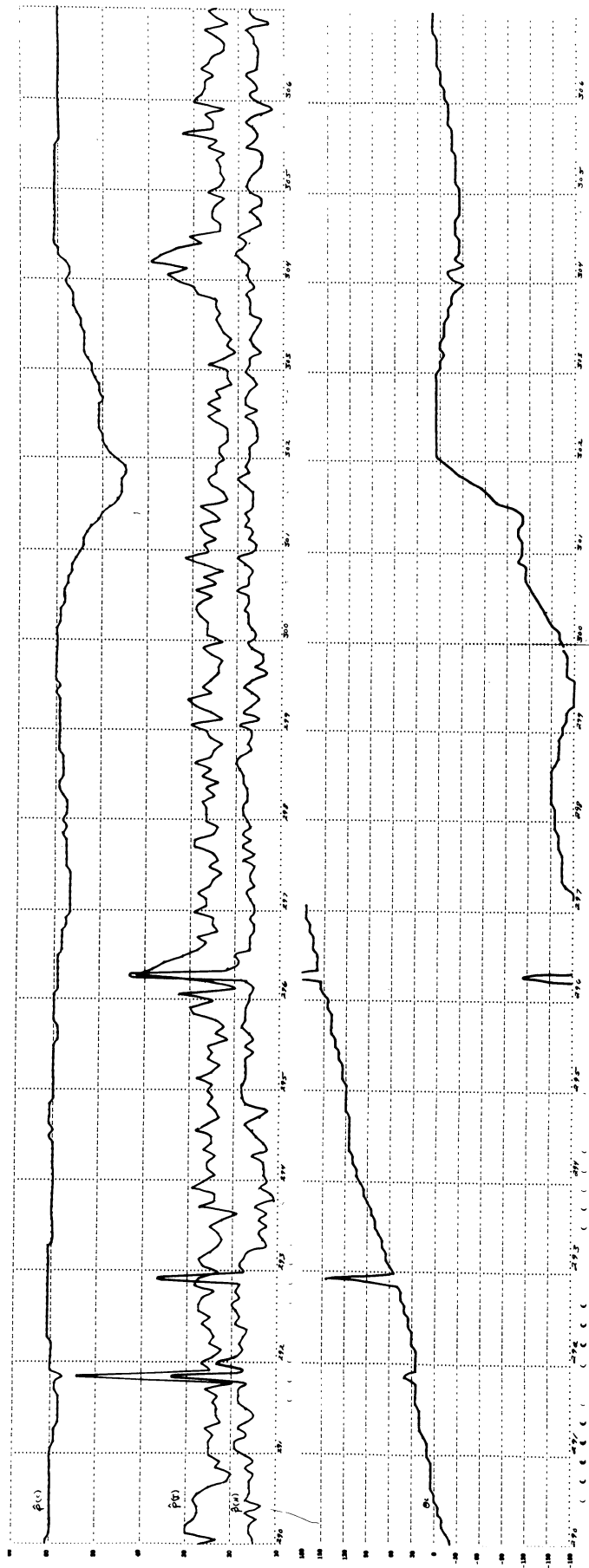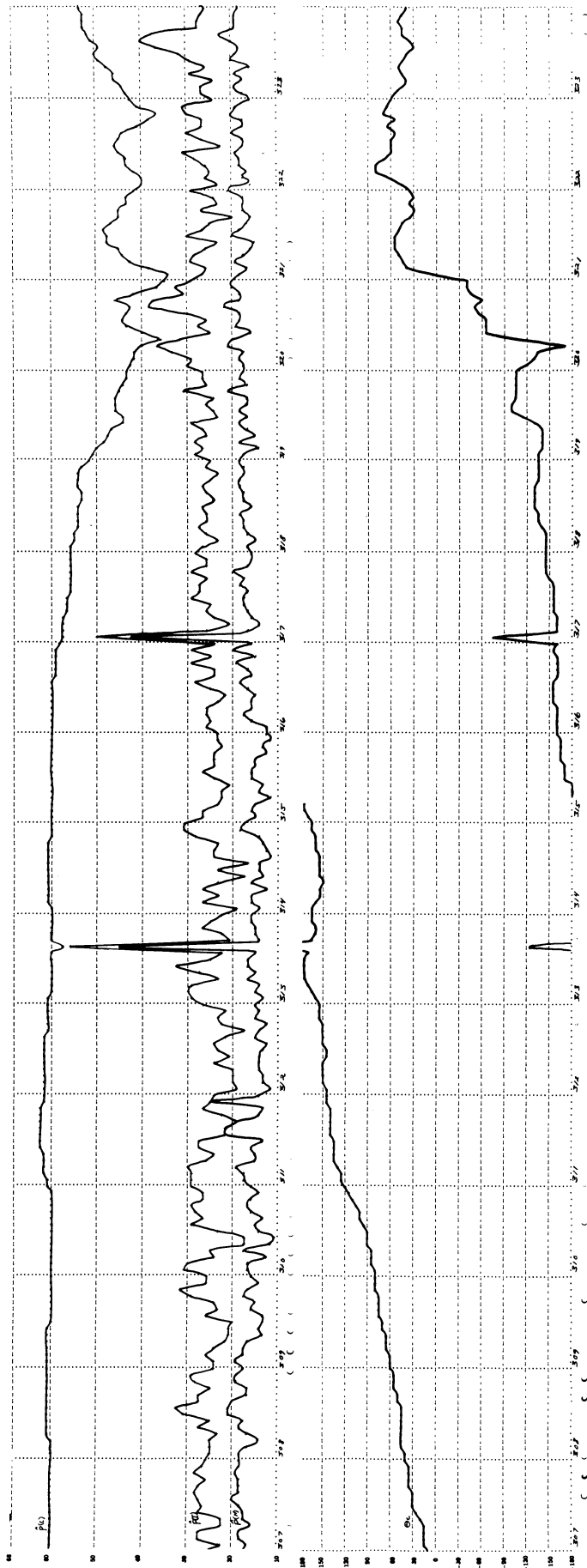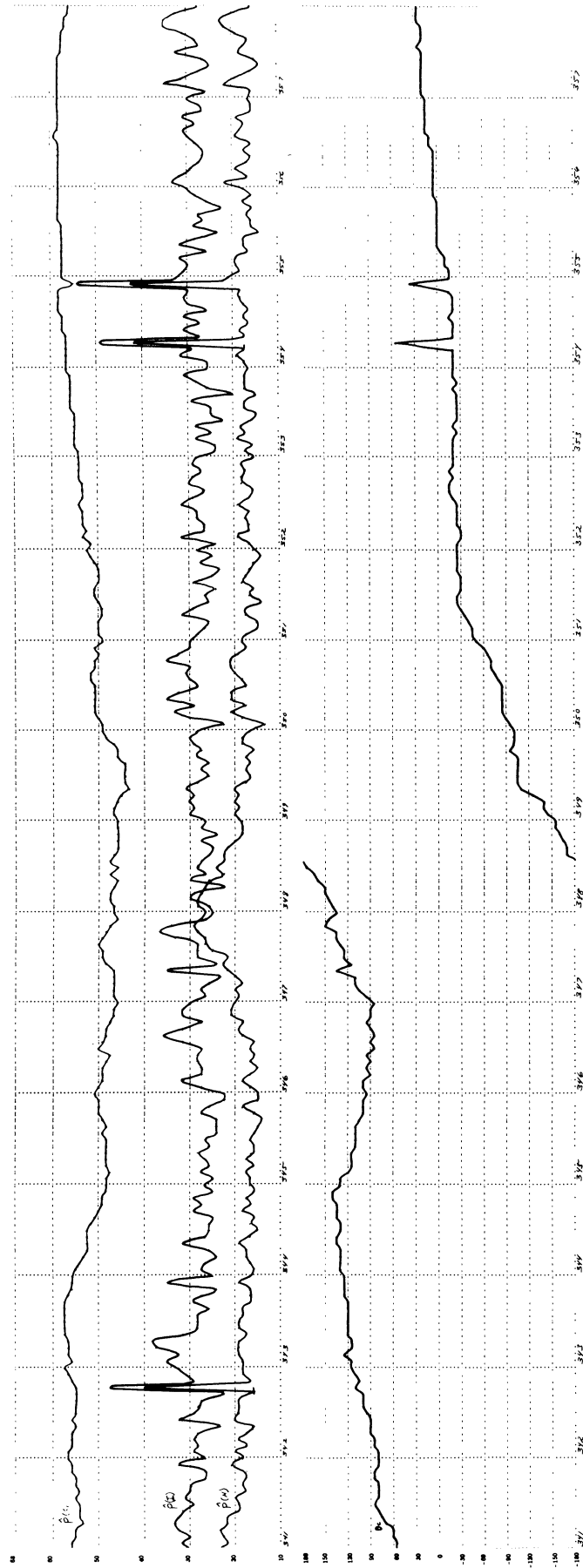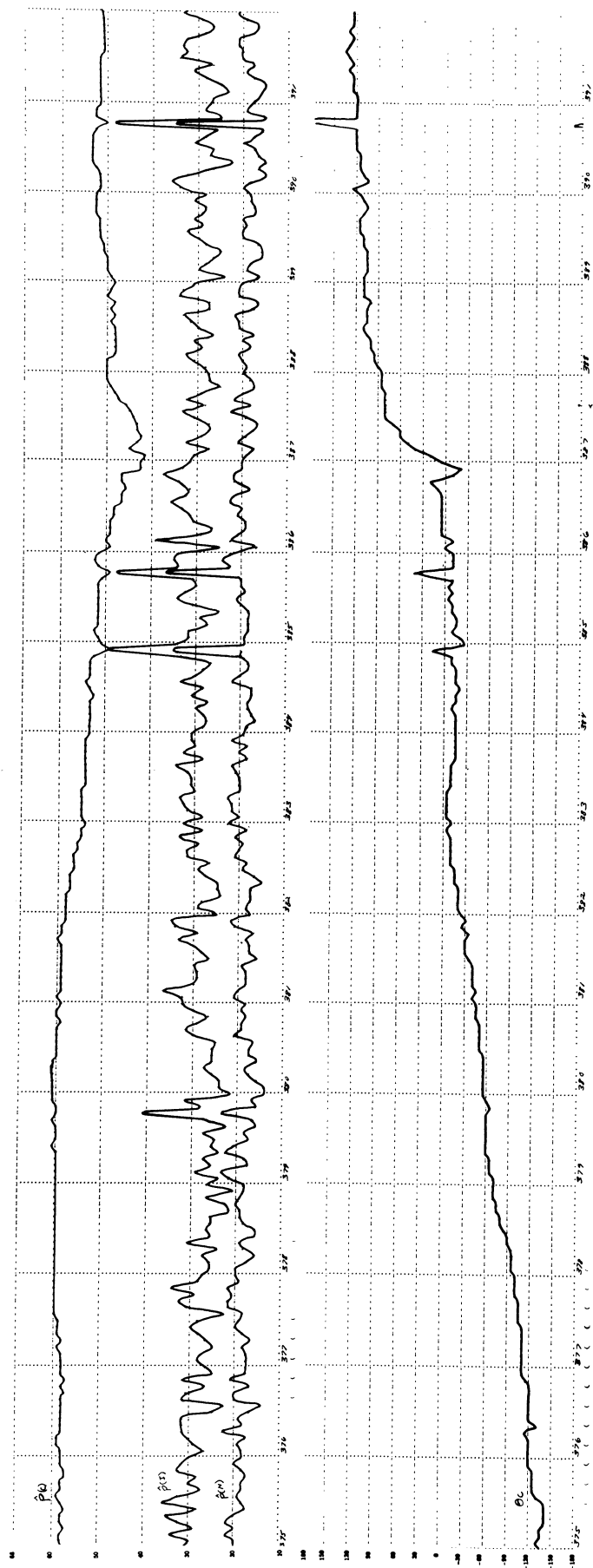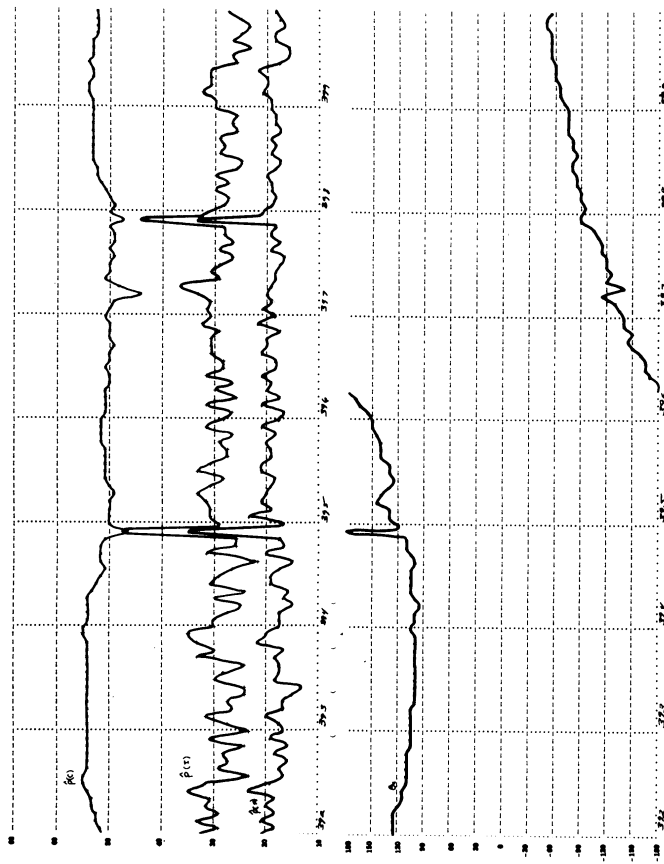
Appendix D

TRIBAND CORRELATION RESULTS

The correlation coefficient is calculated over N points

(N = 56, 126), which corresponds to approximately 28 and 63 minutes

respectively. The coefficients given are between the noise band and

the incoherent band (NI), the coherent band and the incoherent band

(CI), and the noise band and the coherent band (NC).

CORRELATION COEFF. CALC.

ENTER: N=56, T≈28 min
OF BLKS TO CORRELATE 4
OF POINTS OUT 101
STARTING BN 1
OF WORDS/GROUP (MODULUS) 18

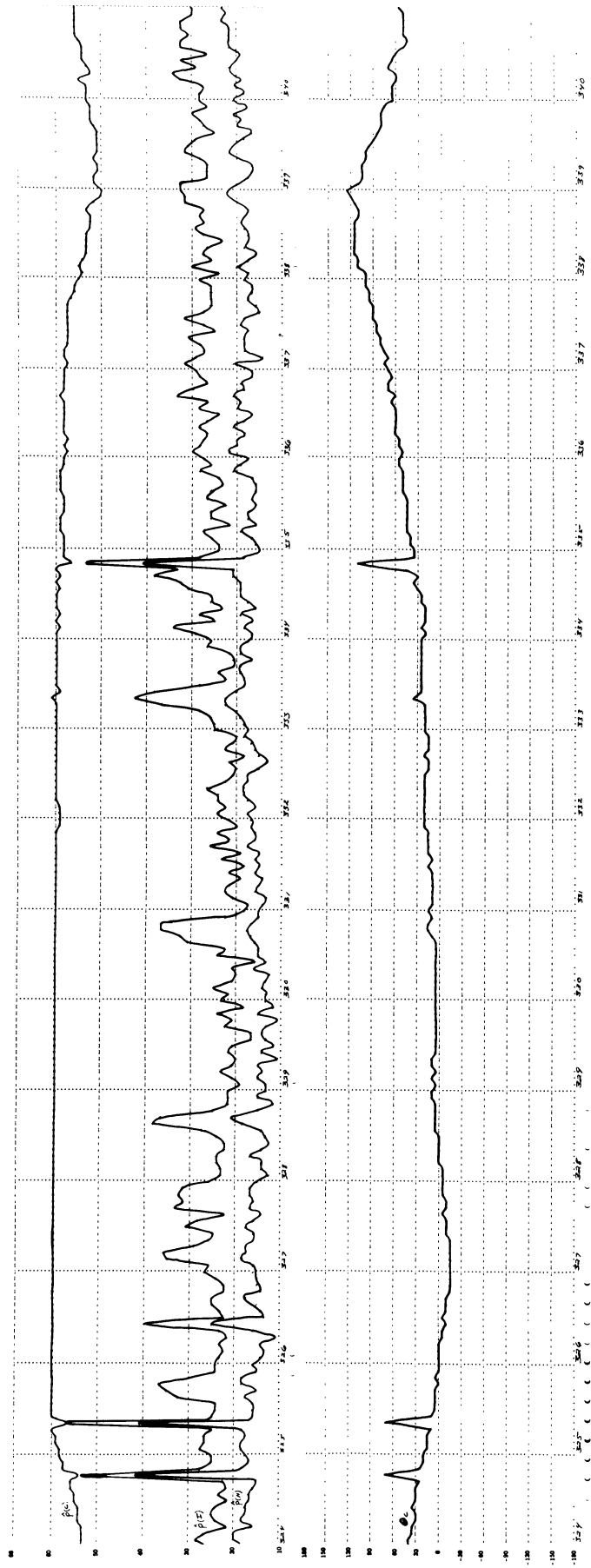| NI	CI	NC
.768221E+00	-.542124E+00	-.733997E+00
.926979E+00	-.775295E+00	-.506757E+00
.957398E+00	.778901E-02	-.270941E+00
.169689E+00	.187681E+00	.365603E+00
.536119E+00	-.182419E+00	.731874E+00
.944009E+00	-.742966E+00	-.510669E+00
.340773E+00	.818059E+00	.517785E+00
-.257064E+00	.604959E+00	.601715E+00
-.434693E+00	-.316658E-02	-.832296E+00
.969706E+00	-.664729E+00	-.611603E+00
.281939E+00	.325287E-01	-.940746E+00
.738934E+00	-.747881E+00	-.435344E+00
.993000E+00	-.452549E+00	-.363563E+00
.949059E+00	.780659E+00	.800856E+00
.999433E+00	.107301E+00	.140699E+00
.960022E+00	.743302E+00	.676333E+00
.555985E+00	.768872E+00	.793511E+00
.917272E+00	-.187870E+00	-.536524E+00
.996137E+00	.652237E+00	.656486E+00
.867264E+00	-.984310E+00	-.771752E+00
.914644E+00	.464299E+00	.701939E+00
.814554E+00	-.289185E-01	-.186831E+00
.851162E+00	-.520266E+00	-.565044E+00
.999722E+00	-.555096E+00	-.544291E+00
.230898E+00	.368665E+00	-.553661E+00
.669264E+00	.473671E+00	-.323476E+00
-.865385E+00	-.339377E+00	.527417E+00
.999689E+00	.337793E+00	.359532E+00
-.701170E+00	.986490E+00	-.731123E+00
.999825E+00	-.441726E+00	-.453521E+00
.614327E+00	-.906397E-01	.384483E-01
.892296E+00	-.452402E+00	-.527684E+00
.661658E+00	.705135E+00	.947424E+00
.973620E+00	.846775E+00	.808879E+00
.988961E+00	-.467819E+00	-.558615E+00
.996962E+00	-.143725E-01	-.658061E-01
.810422E-01	.463479E+00	-.619173E+00
-.323337E+00	.312793E+00	.779649E+00
.997662E+00	.773150E+00	.778983E+00
-.449597E+00	.278002E+00	-.879379E+00
-.871714E+00	.338151E+00	-.278595E+00
.997636E+00	-.466832E+00	-.519870E+00
-.341636E+00	-.588330E+00	-.180242E+00
.999977E+00	-.761135E+00	-.763856E+00
.514344E+00	.681550E+00	.547830E+00
-.116243E+00	.731478E+00	-.486910E+00
.996617E+00	-.966770E+00	-.955783E+00
.979295E+00	.321602E+00	.172914E+00

.726162E+00	.414291E+00	.904994E+00
.999954E+00	.623132E+00	.626142E+00
.380904E+00	-.398644E+00	-.985591E+00
.993480E+00	.574350E+00	.663480E+00
.999989E+00	.798193E+00	.798422E+00
.253791E+00	.120176E+00	.816098E+00
.653909E-01	.870469E+00	-.342827E+00
.966682E+00	.988004E+00	.980031E+00
.854601E+00	.889089E+00	.864674E+00
.978778E+00	.840500E+00	.889653E+00
.656099E-02	.508176E+00	-.569927E+00
.999779E+00	-.516825E+00	-.501038E+00
.978133E+00	.126307E+00	-.781789E-01
.867979E+00	-.215186E+00	-.648876E+00
.944261E+00	.996964E+00	.921924E+00
.972978E+00	.817879E+00	.899589E+00
.466999E+00	.740385E+00	.404221E+00
.996405E+00	-.316869E+00	-.258065E+00
.994249E+00	.345256E+00	.435147E+00
.724201E+00	.812568E+00	.987379E+00
-.660804E+00	-.834162E+00	.181967E+00
-.117367E-01	.822743E+00	.548489E+00
.999196E+00	-.599530E+00	-.573428E+00
.998810E+00	-.634921E+00	-.668882E+00
.120921E+00	-.791588E+00	-.100632E+00
.999732E+00	-.924493E+00	-.918767E+00
-.186241E-01	.252421E+00	-.212692E+00
.784799E+00	.973275E+00	.675830E+00
.713447E+00	.349012E+00	.209448E+00
.494968E+00	-.230740E+00	-.435058E+00
.999989E+00	-.481386E-01	-.506869E-01
.982829E+00	.768324E+00	.848301E+00
.997523E+00	.988864E+00	.976361E+00
.999781E+00	-.894663E+00	-.893824E+00
-.668161E-01	.312382E+00	.444920E+00
.996205E+00	.400714E+00	.319960E+00
.969996E+00	-.188034E+00	-.416844E+00
.955251E+00	.479900E+00	.203257E+00
.235283E+00	.807237E-01	-.927820E+00
.867805E+00	-.372860E-02	-.302750E+00
.999964E+00	-.695337E-01	-.780100E-01
.985296E+00	.825042E+00	.814015E+00
.417991E+00	.993556E+00	.493243E+00
.651386E+00	-.656501E+00	-.103448E+00
.940862E+00	-.740468E+00	-.724225E+00
.997688E+00	-.291692E+00	-.330573E+00
.867174E+00	.181273E+00	-.253211E+00
.979536E+00	-.543909E+00	-.694728E+00
.974991E+00	.924934E+00	.938515E+00
.999840E+00	.184394E+00	.194087E+00
.991547E+00	.132269E+00	.264507E-02
.998893E+00	-.910943E+00	-.916101E+00
-.221869E+00	-.563108E+00	.358225E+00

CORRELATION COEFF. CALC.

ENTER:
OF BLKS TO CORRELATE 9
OF POINTS OUT 45
STARTING BN 1
OF WORDS/GROUP (MODULUS) 18

NI	CI	NC
.852521E+00	-.451818E+00	-.413810E+00
.965293E+00	.452103E+00	.417518E+00
.271267E+00	.486654E+00	.894976E-01
-.219954E+00	.664379E-02	-.262184E+00
.969504E+00	-.421431E+00	-.449434E+00
.992848E+00	-.373550E+00	-.345961E+00
.725915E+00	-.391727E+00	-.448813E-01
.731281E+00	.803340E+00	.882236E+00
.950645E+00	-.462754E-01	.461742E-01
.719960E+00	-.160394E+00	-.358782E+00
.999403E+00	-.365771E+00	-.375217E+00
.438516E+00	-.440403E-01	.322034E+00
.781975E+00	.481732E+00	.405829E+00
.247757E+00	-.120055E+00	.380538E+00
.511026E+00	.248759E+00	.173346E+00
.991362E+00	.196140E+00	.186905E+00
.163457E+00	.353114E+00	.556800E+00
.962848E+00	-.178149E+00	-.166681E+00
.744339E+00	-.305367E+00	.195839E-01
.999921E+00	-.176095E+00	-.172884E+00
.997624E+00	.275327E+00	.283125E+00
.931072E+00	-.297992E-01	-.246240E+00
.909777E+00	-.739983E-01	.771458E-01
.999825E+00	.668380E+00	.678429E+00
.210524E+00	-.824114E-01	-.348032E+00
.978387E+00	.184003E+00	.288743E+00
.794899E+00	-.420493E+00	-.734091E+00
.928913E+00	.213553E+00	.134211E+00
.794454E+00	.361621E+00	.547159E-01
.986533E+00	-.175782E+00	-.492371E-01
-.759288E-01	.444894E+00	.309548E+00
.998951E+00	.273988E+00	.276698E+00
.461461E-01	-.291178E+00	-.243310E+00
.380683E+00	.451562E+00	-.191874E+00
.999869E+00	-.246232E+00	-.250361E+00
.873230E+00	.176823E+00	.289996E+00
.999037E+00	-.800729E+00	-.805181E+00
.917364E+00	.549639E+00	.416587E+00
.240118E-01	.672639E+00	-.291275E+00
.999798E+00	.218474E+00	.212479E+00
.216353E+00	.936935E-01	.138660E+00
.882526E+00	-.434039E+00	-.327080E+00
.893548E+00	-.466099E+00	-.471308E+00
.979042E+00	.196885E+00	.124680E+00
.986949E+00	-.491378E+00	-.388817E+00

REFERENCES

1. Morton Kronengold and William J. Toulis, "Directional 420-Hz Sound Source," IEEE Transactions on Geoscience Electronics, Vol. GE-6, No. 4, November, 1968, pp. 204-24.

2. R. Unger and R. Veenkant, Underwater Sound Propagation in the Straits of Florida: The Mimi Experiment of 3 and 4 February 1965, Technical Report No. 183 (3674-12-T), Cooley Electronics Laboratory, The University of Michigan, Ann Arbor, Michigan, May 1967.

DISTRIBUTION LIST

	No. of Copies
Office of Naval Research (Code 468) Navy Department Washington, D. C. 20360	2
Director, Naval Research Laboratory Technical Information Division Washington, D. C. 20360	6
Director Office of Naval Research Branch Office 1030 East Green Street Pasadena, California 91101	1
Office of Naval Research San Francisco Annex 1076 Mission Street San Francisco, California 94103	1
Office of Naval Research New York Annex 207 West 24th Street New York, New York 10011	1
Director Office of Naval Research Branch Office 219 South Dearborn Street Chicago, Illinois 60604	1
Commanding Officer Office of Naval Research Branch Office Box 39 FPO New York 09510	8
Commander, Naval Ordnance Laboratory Acoustics Division White Oak, Silver Spring, Maryland 20910	1

DISTRIBUTION LIST (Cont.)

	No. of Copies
Commander Naval Ship Systems Command Code SHIPS-03043 Navy Department Washington, D.C. 20360	1
Commander Naval Ship Systems Command Code SHIPS-1630 Navy Department Washington, D.C. 20360	1
Chief Scientist Navy Underwater Sound Reference Division Post Office Box 8337 Orlando, Florida 38200	1
Defense Documentation Center Cameron Station Alexandria, Virginia	20
Dr. Melvin J. Jacobson Rensselaer Polytechnic Institute Troy, New York 12181	1
Dr. Charles Stutt General Electric Company P.O. Box 1088 Schenectady, New York 12301	1
Dr. J. V. Bouyoucos General Dynamics/Electronics 1400 N. Goodman Street P.O. Box 226 Rochester, New York 14609	1
Mr. J. Bernstein EDO Corporation College Point, New York 11356	1

	No. of Copies
Dr. T. G. Birdsall Cooley Electronics Laboratory The University of Michigan Ann Arbor, Michigan 48105	1
Dr. John Steinberg Institute of Marine Science The University of Miami Miami, Florida 33149	1
Dr. R. A. Roberts Department of Electrical Engineering University of Colorado Boulder, Colorado	1
Commander Naval Ordnance Test Station Pasadena Annex 3203 E. Foothill Boulevard Pasadena, California 91107	1
Dr. Stephen Wolff John Hopkins University Baltimore, Maryland 21218	1
Dr. M. A. Basin Litton Industries 8000 Woodley Avenue Van Nuys, California 91409	1
Dr. Albert Nuttall Litton Systems, Inc. 335 Bear Hill Road Waltham, Massachusetts 02154	1
Dr. Philip Stocklin Box 360 Raytheon Company Newport, Rhode Island 02841	1

DISTRIBUTION LIST (Cont.)

	No. of Copies
Dr. H. W. Marsh Raytheon Company P.O. Box 128 New London, Connecticut 06321	1
Mr. Ken Preston Perkin-Elmer Corporation Electro-Optical Division Norwalk, Connecticut 06852	1
Mr. Tom Barnard Texas Instruments Incorporated 100 Exchange Park North Dallas, Texas 75222	1
Dr. John Swets Bolt, Beranek and Newman 50 Moulton Street Cambridge 38, Massachusetts	1
Dr. H. S. Hayre The University of Houston Cullen Boulevard Houston, Texas 77004	1
Dr. Robert R. Brockhurst Woods Hole Oceanographic Institute Woods Hole, Massachusetts	1
Cooley Electronics Laboratory The University of Michigan Ann Arbor, Michigan 48105	50
Director Office of Naval Research Branch Office 495 Summer Street Boston, Massachusetts 02210	1

DISTRIBUTION LIST (Cont.)

14. KEY WORDS	LINK A		LINK B		LINK C	
	ROLE	WT	ROLE	WT	ROLE	WT
Signal Processing						
Acoustic Propagation						
Digital Filtering						

DD FORM 1 NOV 65 **1473** (BACK)

S/N 0101-807-6821

DOCUMENT CONTROL DATA - R & D

(Security classification of title, body of abstract and indexing annotation must be entered when the overall report is classified)

1. ORIGINATING ACTIVITY *(Corporate author)*	2a. REPORT SECURITY CLASSIFICATION
Cooley Electronics Laboratory The University of Michigan Ann Arbor, Michigan 48105	Unclassified
	2b. GROUP

3. REPORT TITLE

Triband: The Three Band Filter for the Continuing MIMI Experiment

4. DESCRIPTIVE NOTES *(Type of report and inclusive dates)*

Technical Report No. 201 - 03674-24-T

5. AUTHOR(S) *(First name, middle initial, last name)*

Hatter, Norman

6. REPORT DATE	7a. TOTAL NO. OF PAGES	7b. NO. OF REFS
February 1970	102	2

8a. CONTRACT OR GRANT NO. Nonr-1224(36) b. PROJECT NO. NR187-200 c. d.	9a. ORIGINATOR'S REPORT NUMBER(S) 03674-24-T 9b. OTHER REPORT NO(S) *(Any other numbers that may be assigned this report)* TR 201

10. DISTRIBUTION STATEMENT

Reproduction in whole or in part is permitted for any purpose of the U.S. Government.

11. SUPPLEMENTARY NOTES	12. SPONSORING MILITARY ACTIVITY Office of Naval Research Department of the Navy Washington, D.C. 20360

13. ABSTRACT

An experiment was conducted as part of the continuing study of sound propagation in the Straits of Florida. A 420-Hz continuous wave (CW) signal was transmitted, received at the 7-mile hydrophone, and processed by the Linc-8 on-line digital processor. The processing yielded the magnitude and phase of the reception in a 1/16-Hz band, the magnitude of the reception in a 1-Hz band but excluding the 1/16-Hz band, and the magnitude of the reception in a 16-Hz band that excluded the 1-Hz band. All bands were centered at 420 Hz. The purposes of the experiment were to verify the possibility of such a three-band analysis and to obtain "typical" relative power ratios to aid in the design of analog triband phase coherent demodulation.

DD FORM 1473 (PAGE 1)
1 NOV 65

S/N 0101-807-6811

A-31408